

Incommensurate magnetic states induced by ordering competition in $\text{Ba}_{1-x}\text{Na}_x\text{Fe}_2\text{As}_2$

Jing Wang*

Department of Physics, Tianjin University, Tianjin 300072, P.R. China

(Dated: November 11, 2022)

Quantum criticality nearby a certain magnetic phase transition beneath the superconducting dome of $\text{Ba}_{1-x}\text{Na}_x\text{Fe}_2\text{As}_2$ is attentively studied by virtue of a phenomenological theory in conjunction with renormalization group approach. We report that ordering competition between magnetic and superconducting fluctuations is capable of coaxing incommensurate (IC) magnetic states to experience distinct fates depending upon their spin configurations. The C_2 -symmetry IC magnetic stripe with perpendicular magnetic helix dominates over other C_2 -symmetry magnetic competitors and hints at a potential candidate for the unknown C_2 -symmetry magnetic state. Amongst C_4 -symmetry IC magnetic phases, IC charge spin density wave is substantiated to be superior, shedding light on the significant intertwining of charge and spin degrees of freedom. Meanwhile, ferocious fluctuations render a sharp fall of superfluid density alongside dip of critical temperature as well as intriguing behavior of London penetration depth.

PACS numbers: 74.70.-b, 74.20.De, 74.25.Dw, 74.62.-c

I. INTRODUCTION

The last dozen years have witnessed considerably intense research devoted to iron pnictides of BaFe_2As_2 family [1–13], whose phase diagrams are ubiquitously borne out of both superconducting (SC) and diverse kinds of magnetic orders mediated by quantum phase transitions (QPTs) [14]. Notwithstanding magnetism is an antagonistic state versus superconductivity, they compete and collaborate other than coexist with each other [12, 13, 15]. This accordingly poses a substantial challenge as to what the connection is between magnetic and SC states, providing a crucial ingredient to glue Cooper pairing [12, 13]. In the light of abundant magnetic states in BaFe_2As_2 [4–11], one of the most imperative and realistic quests of understanding this very compound, prior to exploring the ultimate SC nature, is how to unambiguously identify concrete configurations of magnetic states around QPTs in that different states are associated with distinguished fluctuations which play a pivotal role in establishing its phase diagram.

Instead of global scenario, the focus of this paper is on finding specific magnetic states that reside close to magnetic QPTs in the phase diagram of $\text{Ba}_{1-x}\text{Na}_x\text{Fe}_2\text{As}_2$ [4, 5, 8–10]. This compound provides a versatile platform to investigate ordering-competition impacts on stabilities of magnetic states and relations with SC state. On one hand, it hosts a rather rich phase diagram with typical doping-tuned magnetic QPTs compared to other BaFe_2As_2 systems. It is of unique interest to asseverate there exists an elusive C_2 -symmetry (C_2) magnetic phase in Na-doped system reported recently by Wang *et al.* [8], which is hitherto enigmatic and remains an open topic. On the other, three commensurate plus kinds of IC magnetic states might all be possible candidates inhabiting in

its phase diagram [5, 6, 16–19]. To be specific, the commensurate magnetic states involve the stripe spin density wave (SDW), charge spin density wave (CSDW), and spin vortex crystal (SVC) [16, 17, 33, 34]. In addition, the IC magnetic states cover four different C_2 -symmetry (C_2) IC cases consisting of C_2 IC stripe (ICS), C_2 magnetic helix (MH), C_2 IC magnetic stripe with perpendicular magnetic helix ($\text{ICS} \perp \text{MH}$), and C_2 double parallel magnetic helix (DPMH), as well as three distinct C_4 -symmetry (C_4) IC situations involving C_4 IC CSDW, C_4 IC SVC, and C_4 IC spin-whirl crystal (SWC) [19]. Due to their own peculiarities, these distinct states conventionally bring forward various outcomes. Questions are naturally raised: which one is the prime C_4 -symmetry (C_4) magnetic order in the shadow of some QPT and what is the optimal state characterizing the mystic C_2 magnetic state? We respond by taking advantage of a phenomenological theory together with the Wilsonian renormalization group (RG) [20]. The answers are of notable help to deeply understand the phase diagram and even offer instructive insights into pairing mechanism. Fig. 1 schematically illustrates our central results driven by ordering competition.

The rest of paper is organized as follows. In Sec. II, we establish the phenomenological effective theory and provide the coupled RG equations after performing the one-loop momentum-shell RG analysis. Next, within Sec. III we endeavor to select the most favorable IC SDW states among all potential candidates under the influence of strong quantum fluctuations induced by the QCP. Sec. IV is accompanied by an investigation of unusual physical implications including both superfluid density and London penetration depth caused by the ferocious ordering competition near the QCP. Finally, we briefly summarize the primary conclusions in Sec. V.

*E-mail address: jing_wang@tju.edu.cn

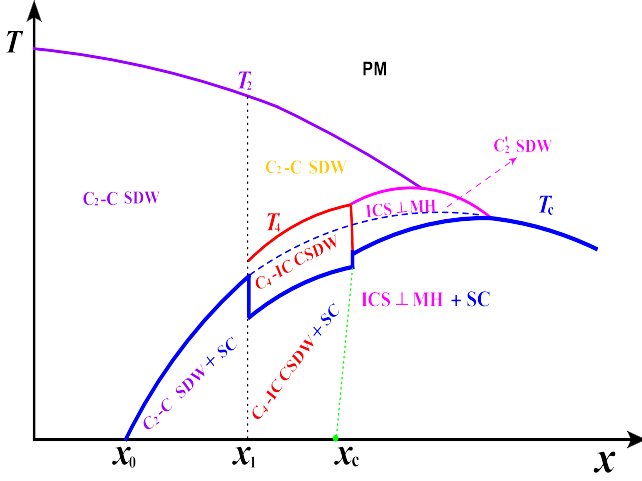


FIG. 1: (Color online) Schematic $x - T$ phase diagram of $\text{Ba}_{1-x}\text{Na}_x\text{Fe}_2\text{As}_2$ in the vicinity of a vital magnetic quantum critical point (QCP) located at x_c . PM, SDW, and SC are shortened notations for paramagnetism, spin density wave (SDW), and superconductivity with $T_{2,4}$ and T_c denoting the critical temperatures from PM to $C_{2,4}$ SDW and non-SC to SC, respectively. Ordering competition under the ferocious quantum fluctuations bears out that C_2 ICS \perp MH state is a good candidate for the cryptic C_2 magnetic state (C_2' SDW) and the leading C_4 SDW close by the QCP is preferable to be an IC CSDW, which are manifestly substantiated and supported by the combination of Table I and Fig. 6. Instead, other potential candidates, including C_2 ICS, DPMH, and MH SDW states as well as C_4 IC SVC and SWC states, cannot survive in the neighboring regime of the QCP as addressed in Appendix B (the abbreviations of states hereby are consistent with those in Table I's).

II. EFFECTIVE THEORY AND RG ANALYSIS

A. Effective theory

The fermi surfaces of BaFe_2As_2 compounds under a three-band model consist of one hole pocket at the center of Brillouin zone $\mathbf{Q}_\Gamma = (0, 0)$ and two electron pockets centered at two fixed momenta $\mathbf{Q}_X = (\pi, 0)$ and $\mathbf{Q}_Y = (0, \pi)$ [13, 21–23]. From microscopical considerations, both magnetic and SC states are rooted in interactions among excited quasiparticles from these Fermi pockets [13, 16, 17, 21–24]. Concretely, a magnetic state is composed of two basic magnetic order parameters \mathbf{M}_X and \mathbf{M}_Y , which are designated by $\mathbf{M}_j = \sum_{\mathbf{k}} c_{\Gamma, \mathbf{k}\alpha}^\dagger \vec{\sigma}_{\alpha\beta} c_{j, \mathbf{k}+\mathbf{Q}_j\beta}$ with $j = X, Y$ [22–26]. To involve

IC magnetic states, ordering vectors are afterwards distributed as $\mathbf{Q}_X = (\pi - \delta, 0)$ and $\mathbf{Q}_Y = (0, \pi - \delta)$ with δ being a small correction for generic wavevectors. This indicates that the magnetic order parameters are regarded as a complex quantity $M_{\mathbf{Q}_{X,Y}} \neq M_{\mathbf{Q}_{X,Y}}^* \equiv M_{-\mathbf{Q}_{X,Y}}$, which is in striking contrast to the commensurate case with $\delta = 0$ and $M_{\mathbf{Q}_{X,Y}}^* = M_{\mathbf{Q}_{X,Y}}$ [16, 17, 19].

We begin with the extended Landau-Ginzburg free energy after integrating out the fermionic ingredients [16, 17, 19, 27, 28]

$$f = \alpha(|\mathbf{M}_X|^2 + |\mathbf{M}_Y|^2) + \frac{\beta_2}{2}(|\mathbf{M}_X|^2 + |\mathbf{M}_Y|^2)^2 + \frac{\beta_1 - \beta_2}{2}(|\mathbf{M}_X^2|^2 + |\mathbf{M}_Y^2|^2) + (g_1 - \beta_2)|\mathbf{M}_X|^2|\mathbf{M}_Y|^2 + \frac{g_2}{2}(|\mathbf{M}_X \cdot \mathbf{M}_Y|^2 + |\mathbf{M}_X \cdot \mathbf{M}_Y^*|^2), \quad (1)$$

with α , $\beta_{1,2}$, and $g_{1,2}$ being fundamental structure parameters. It deserves to be pointed out that the QCP at x_1 in Fig. 1 associated with commensurate states was studied previously [16–18]. In order to determine the unknown C_2 and C_4 IC SDWs, we hereafter concentrate on the magnetic QPT denoted by x_c in Fig. 1.

After designating $\mathbf{M}_X \equiv M_X \cos \theta \mathbf{n}_X$ and $\mathbf{M}_Y \equiv M_Y \sin \theta \mathbf{n}_Y$, where $\theta \in (0, \pi/2)$ and $|\mathbf{n}_{X,Y}|^2 = 1$ specify the spin configurations of magnetic states, we go beyond mean-field level and construct a phenomenological effective field theory [16, 22], which captures main information of ordering competition including both $C_{2,4}$ -symmetric IC magnetic and SC fluctuations [18, 29–31]. To this end, the phenomenological effective action [16, 22] can be casted as

$$S = \int d^d \mathcal{L} = \int d^d \mathcal{L}_{\text{SDW}} + \int d^d \mathcal{L}_{\text{SC}} + \int d^d \mathcal{L}_{\text{SDW-SC}}, \quad (2)$$

where \mathcal{L}_{SDW} , \mathcal{L}_{SC} , and $\mathcal{L}_{\text{SDW-SC}}$ correspond to SDW, SC orders, and their interplay, respectively.

At first, we examine \mathcal{L}_{SDW} . An angle $\theta \in [0, \pi/2]$ is employed to specify the direction of magnetic order parameter \mathbf{M} in the spin space. Accordingly, the order parameter can be divided into two components $\mathbf{M}_X \equiv M_X \cos \theta \mathbf{n}_X$ and $\mathbf{M}_Y \equiv M_Y \sin \theta \mathbf{n}_Y$ by projecting \mathbf{M} onto the spin vectors \mathbf{n}_X and \mathbf{n}_Y , which characterize the spin configurations of magnetic states with $|\mathbf{n}_{X,Y}|^2 = 1$ and whose concrete values depending upon the types of candidate states [19]. Inserting them into the free energy density (1) by adding the dynamical terms of magnetic order parameters then gives rise to [16, 18, 22, 27]

$$\begin{aligned} \mathcal{L}_{\text{SDW}} = & \left[|\mathbf{n}_X \cos \theta|^2 \frac{1}{2} (\partial_\mu M_X)^2 + \alpha (|\mathbf{n}_X|^2 \cos^2 \theta) M_X^2 \right] + \left[|\mathbf{n}_Y \sin \theta|^2 \frac{1}{2} (\partial_\mu M_Y)^2 + \alpha (|\mathbf{n}_Y|^2 \sin^2 \theta) M_Y^2 \right] \\ & + \frac{\beta_1 - \beta_2}{2} (|\mathbf{n}_X^2|^2 \cos^4 \theta M_X^4 + |\mathbf{n}_Y^2|^2 \sin^4 \theta M_Y^4) + \frac{\beta_2}{2} (|\mathbf{n}_X|^4 \cos^4 \theta M_X^4 + |\mathbf{n}_Y|^4 \sin^4 \theta M_Y^4) \\ & + g_1 |\mathbf{n}_X|^2 |\mathbf{n}_Y|^2 \cos^2 \theta \sin^2 \theta M_X^2 M_Y^2 + \frac{g_2}{2} \cos^2 \theta \sin^2 \theta (|\mathbf{n}_X \cdot \mathbf{n}_Y|^2 + |\mathbf{n}_X \cdot \mathbf{n}_Y^*|^2) M_X^2 M_Y^2. \end{aligned} \quad (3)$$

We next consider \mathcal{L}_{SC} . In order to obtain SC fluctuations in the ordered state, we bring out the the following contribution by employing the condition $\partial_\mu A_\mu = 0$ [29]

$$\mathcal{L}_{\text{SC}} = \partial_\mu \Delta^\dagger \partial_\mu \Delta + a_s \Delta^2(k) + \frac{u_s}{2} \Delta^4(k) + \frac{\alpha_A}{2} A^2 - \frac{1}{4} (\partial_\mu A_\nu - \partial_\nu A_\mu)^2 + \lambda_{\Delta A} |\Delta|^2 A^2. \quad (4)$$

As the system enters the SC ordered state around the SDW QCP, we need to expand the SC order parameter by introducing two new gapless fields

$$\Delta = V_0 + \frac{(h + i\eta)}{\sqrt{2}}, \langle h \rangle = \langle \eta \rangle = 0, V_0 \equiv \langle \Delta \rangle = \sqrt{\frac{-a_s}{u_s}}, \quad (5)$$

which help us to extract the potential fluctuation of SC order parameter [30], to make the \mathbf{A} massive after absorbing the gapless Goldstone particles. Combing Eq. (4) and Eq. (5), after discarding the constant terms and choosing some transformation to make $\eta = 0$ due to the

local gauge invariance [30], we obtain

$$\begin{aligned} \mathcal{L}_{\text{SC}} = & \frac{1}{2} (\partial_\mu h)^2 - a_s h^2 + \frac{u_s}{8} h^4 + \frac{\sqrt{-2a_s u_s}}{2} h^3 \\ & - \frac{1}{4} (\partial_\mu A_\nu - \partial_\nu A_\mu)^2 + \frac{\alpha_A}{2} A^2 \\ & + \lambda_{\Delta A} \sqrt{\frac{-2a_s}{u_s}} h A^2 + \frac{\lambda_{\Delta A}}{2} h^2 A^2, \end{aligned} \quad (6)$$

where the “mass” of field A is defined as $\alpha_A \equiv \lambda_{\Delta A} \frac{-2a_s}{u_s}$.

Finally, we introduce \mathcal{L}_{SC} . The interplay between SC and SDW order parameters can be written as [18],

$$\mathcal{L}_{\text{SDW-SC}} = \lambda(|\mathbf{M}_X|^2 + |\mathbf{M}_Y|^2) \Delta^2 + \kappa(|\mathbf{M}_X \cdot \mathbf{M}_Y| + |\mathbf{M}_X \cdot \mathbf{M}_Y^*|) \Delta^2. \quad (7)$$

Based on the information of \mathcal{L}_{SDW} and \mathcal{L}_{SC} , we are left with our effective theory

$$\begin{aligned} \mathcal{L}_{\text{eff}} = & \left[\frac{1}{2} (\partial_\mu M_X / \mathcal{C})^2 + \alpha_X M_X^2 + \frac{\beta_X}{2} M_X^4 \right] + \left[\frac{1}{2} (\partial_\mu M_Y / \mathcal{S})^2 + \alpha_Y M_Y^2 + \frac{\beta_Y}{2} M_Y^4 \right] + \left[-\frac{1}{4} (\partial_\mu A_\nu - \partial_\nu A_\mu)^2 + \frac{\alpha_A}{2} A^2 \right] \\ & + \left[\frac{1}{2} (\partial_\mu h)^2 + a_h h^2 + \frac{\beta_h}{2} h^4 + \gamma_h h^3 \right] + \alpha_{XY} M_X M_Y + \gamma_{XYh} M_X M_Y h + \gamma_{X^2h} M_X^2 h + \gamma_{Y^2h} M_Y^2 h + \gamma_{hA^2} h A^2 \\ & + \lambda_{XY} M_X^2 M_Y^2 + \lambda_{Xh} M_X^2 h^2 + \lambda_{Yh} M_Y^2 h^2 + \lambda_{XYh} M_X M_Y h^2 + \lambda_{hA} h^2 A^2, \end{aligned} \quad (8)$$

with $\mathcal{C} \equiv 1/|\mathbf{n}_X \cos \theta|^2$ and $\mathcal{S} \equiv 1/|\mathbf{n}_Y \sin \theta|^2$. $M_{X,Y}$ point to magnetic fluctuations and h, A are auxiliary fields to absorb SC fluctuations. We here dub factors in (8) such as α_X etc. the effective parameters to pre-

vent them from being confused with fundamental parameters appearing in Eq. (1). Two series of parameters are bridged by virtue of following relationships,

$$\alpha_h \equiv (-a_s), \beta_h \equiv \frac{u_s}{4}, \gamma_h \equiv \frac{\sqrt{-2a_s u_s}}{2}, \alpha_A \equiv \frac{-2\lambda_{\Delta A} a_s}{u_s}, \gamma_{hA^2} \equiv \lambda_{\Delta A} \sqrt{\frac{-2a_s}{u_s}}, \lambda_{hA} \equiv \frac{\lambda_{\Delta A}}{2}, \quad (9)$$

$$\alpha_X \equiv \left(a - \frac{\lambda a_s}{u_s} \right) (|\mathbf{n}_X|^2 \cos^2 \theta), \beta_X \equiv \beta_2 (|\mathbf{n}_X|^4 \cos^4 \theta) + (\beta_1 - \beta_2) (|\mathbf{n}_X^2|^2 \cos^4 \theta), \quad (10)$$

$$\alpha_Y \equiv \left(a - \frac{\lambda a_s}{u_s} \right) (|\mathbf{n}_Y|^2 \sin^2 \theta), \beta_Y \equiv \beta_2 (|\mathbf{n}_Y|^4 \sin^4 \theta) + (\beta_1 - \beta_2) (|\mathbf{n}_Y^2|^2 \sin^4 \theta), \quad (11)$$

$$\alpha_{XY} \equiv \frac{-a_s \kappa}{u_s} (|\cos \theta \sin \theta \mathbf{n}_X \cdot \mathbf{n}_Y| + |\cos \theta \sin \theta \mathbf{n}_X \cdot \mathbf{n}_Y^*|), \quad (12)$$

$$\gamma_{XYh} = \kappa \sqrt{\frac{-2a_s}{u_s}} (|\cos \theta \sin \theta \mathbf{n}_X \cdot \mathbf{n}_Y| + |\cos \theta \sin \theta \mathbf{n}_X \cdot \mathbf{n}_Y^*|), \quad (13)$$

$$\gamma_{X^2h} \equiv \lambda \sqrt{\frac{-2a_s}{u_s}} (|\mathbf{n}_X|^2 \cos^2 \theta), \gamma_{Y^2h} \equiv \lambda \sqrt{\frac{-2a_s}{u_s}} (|\mathbf{n}_Y|^2 \sin^2 \theta), \quad (14)$$

$$\lambda_{XY} \equiv g_1 \cos^2 \theta \sin^2 \theta (|\mathbf{n}_X|^2 |\mathbf{n}_Y|^2) + \frac{g_2}{2} \cos^2 \theta \sin^2 \theta (|\mathbf{n}_X \cdot \mathbf{n}_Y|^2 + |\mathbf{n}_X \cdot \mathbf{n}_Y^*|^2), \quad (15)$$

$$\lambda_{Xh} \equiv \frac{\lambda}{2} (|\mathbf{n}_X|^2 \cos^2 \theta), \lambda_{Yh} \equiv \frac{\lambda}{2} (|\mathbf{n}_Y|^2 \sin^2 \theta), \quad (16)$$

$$\lambda_{XYh} \equiv \frac{\kappa}{2} (|\cos \theta \sin \theta \mathbf{n}_X \cdot \mathbf{n}_Y| + |\cos \theta \sin \theta \mathbf{n}_X \cdot \mathbf{n}_Y^*|), \quad (17)$$

where κ and $\lambda_{\Delta A}$ cannot be represented by original parameters a , a_s , u_s , λ , β_1 , β_2 , g_1 , and g_2 appearing in the free energy (1), and therefore comes up with two supplementary fundamental parameters. It is necessary to point out these effective parameters are intermediate auxiliary variables but instead the fundamental parameters play a central role in pinning down the specific SDW states.

B. RG analysis

As aforementioned in Sec. II A, the concrete spin configuration state would be essentially determined by the fundamental parameters. In order to examine the stabilities of all potential states, we need to construct the energy-dependent coupled RG equations of the fundamental parameters. To this end, we compute one-loop corrections to all effective parameters in Eq. (8) and derive the corresponding RG evolutions within Wilsonian RG framework [18, 20, 31] via integrating out the fast fields in the momentum shell $e^{-l}\Lambda < k < \Lambda$ with the running scale $l > 0$. Since the fundamental parameters defined in Eq. (1) dictate the physical properties, it heralds undeviatingly that a pillar of task consists in refining their flow equations. To this end, we resort to the strategy in Refs. [18, 31]. Combining RG flows of effective parameters and connections with fundamental parameters (9)-(17) yields a set of coupled RG equations

$$\frac{d\mathcal{X}_i}{dl} = \sum_j \mathcal{F}_{ij}\mathcal{X}_j, \quad (18)$$

with $\mathcal{X}_{i/j}$ serving as the fundamental parameters [32] and \mathcal{F}_{ij} standing for evolution coefficients as a function of $\mathcal{X}_{i/j}$. This necessitates bearing in mind that the coupled RG evolutions hinge heavily upon the spin configurations of magnetic fluctuations, namely the relationships between $|\mathbf{n}_X|^2$, $|\mathbf{n}_X|^4$, $|\mathbf{n}_Y|^2$, and $|\mathbf{n}_Y|^4$, which give rise to seven independent classes of RG evolutions. The details of Eq. (18) are stored completely in Appendix A.

III. STABILITIES OF INCOMMENSURATE MAGNETIC STATES

With the help of energy-dependent flows of fundamental parameters, we are now in a suitable situation to study the stabilities of IC magnetic states triggered by some magnetic QCP. As to BaFe_2As_2 compounds, many experimental efforts [4–11] corroborate that magnetism occupies major space of phase diagram in terms of various states with distinguished symmetries and spin configurations. In particular, compound $\text{Ba}_{1-x}\text{Na}_x\text{Fe}_2\text{As}_2$ [5, 8–10] harbors a complicated but fascinating phase diagram sketched in Fig. 1, indicating a string of magnetic states for both C_2 and C_4 symmetries are allowed with proper

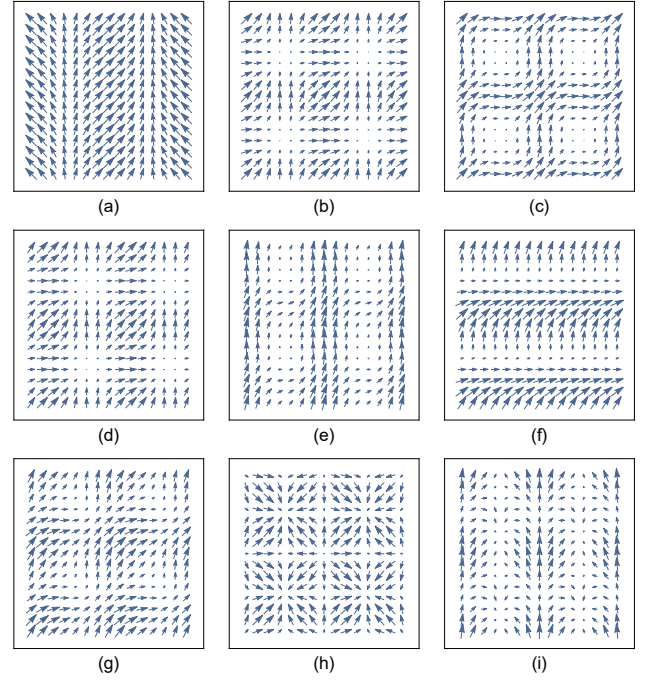


FIG. 2: (Color online) Schematic profile illustrations for nine distinct types of IC spin configurations (at the starting point of RG flows) [19]: (a) C_2 ICS, (b) C_4 IC CSDW, (c) C_4 IC SVC, (d) C_2 IC MH, (e) C_2 ICS \parallel MH, (f) C_2 ICS \perp MH, (g) C_2 IC DPMH, (h) C_4 IC SWC, and (i) C_2 IC SWC.

variations of temperature and doping. Besides three commensurate states, i.e., stripe spin density wave (SSDW), charge spin density wave (CSDW), and spin vortex crystal (SVC) [16, 17, 33, 34], Christensen *et al.* [19] recently advocated that potential IC magnetic states are clustered into nine inequivalent breeds. Moreover, seven of them can be realized with confined parameters of mean-field free energy in the phase diagram [19], which cover four kinds of C_2 IC cases involving C_2 IC stripe (ICS), C_2 magnetic helix (MH), C_2 IC magnetic stripe with perpendicular magnetic helix (ICS \perp MH), and C_2 double parallel magnetic helix (DPMH), as well as three distinct C_4 IC situations consisting of C_4 IC CSDW, C_4 IC SVC, and C_4 IC spin-whirl crystal (SWC). Their spin configurations as well as their stability constraints and final fates are catalogued point-to-point in Table I. In order to roughly capture the structural information of distinct types of SDW states, Fig. 2 presents the relevant schematic illustrations of related spin configurations for potential IC magnetic states.

A. Setup and Strategy

Despite being an underlying antagonist against SC state, magnetism is assumed to be of intimate relevance to superconductivity as they are closely adjacent to each other or even coexist near the magnetic QPT. To be con-

TABLE I: Collections of low-energy fates for IC magnetic states in $\text{Ba}_{1-x}\text{Na}_x\text{Fe}_2\text{As}_2$. The first line enumerates seven distinguished types of IC magnetic states as well as the second and third lines provide their related spin configurations and schematic illustrations, respectively. In addition, the fourth line shows stable constraints as functions of fundamental interaction parameters [19] and the last line presents the corresponding low-energy stabilities. Herein, ✓ and ✗ stand for a stable state (i.e., the prevailing candidate by the side of the magnetic QCP) and an unstable state, respectively.

IC magnetic states	ICS	MH	ICS \perp MH	DPMH	IC CSDW	IC SVC	SWC
Spin configurations	$\mathbf{n}_X = (0, 0, 1), \mathbf{n}_Y = (0, 0, 0)$	$\mathbf{n}_X = \frac{1}{\sqrt{2}}(i, 0, 1), \mathbf{n}_Y = (0, 0, 0)$	$\mathbf{n}_X = (0, 0, 1), \mathbf{n}_Y = \frac{1}{\sqrt{2}}(i, 1, 0)$	$\mathbf{n}_X = \mathbf{n}_Y = \frac{1}{\sqrt{2}}(i, 0, 1)$	$\mathbf{n}_X = (0, 0, 1), \mathbf{n}_Y = (0, 0, 1)$	$\mathbf{n}_X = (0, 0, 1), \mathbf{n}_Y = (0, 1, 0)$	$\mathbf{n}_X = \frac{1}{\sqrt{2}}(i, 0, 1), \mathbf{n}_Y = \frac{1}{\sqrt{2}}(0, i, 1)$
Schematic illustrations	Fig. 2(a)	Fig. 2(d)	Fig. 2(f)	Fig. 2(g)	Fig. 2(b)	Fig. 2(c)	Fig. 2(h)
Stable constraints	$\beta_1 - \beta_2 < 0$ with $\frac{g_2}{ \beta_1 - \beta_2 } > 0$, $\frac{g_1 - \beta_2}{ \beta_1 - \beta_2 } > -1$ or $\frac{g_2}{ \beta_1 - \beta_2 } < 0$, $\frac{g_1 - \beta_2 - 0.9g_2}{ \beta_1 - \beta_2 } > -1$	$\beta_1 - \beta_2 > 0$ with $\frac{g_2}{ \beta_1 - \beta_2 } > 0$, $\frac{g_1 - \beta_2}{ \beta_1 - \beta_2 } > 0$ or $\frac{g_2}{ \beta_1 - \beta_2 } < 0$, $\frac{g_1 - \beta_2 - 0.9g_2}{ \beta_1 - \beta_2 } > -1$	$\beta_1 - \beta_2 > 0$, $\frac{g_2}{ \beta_1 - \beta_2 } > 2$, $\frac{g_1 - \beta_2}{ \beta_1 - \beta_2 } < 0$	$\beta_1 - \beta_2 > 0$, $\frac{g_2}{ \beta_1 - \beta_2 } < 0$, $\frac{g_1 - \beta_2 - 0.9g_2}{ \beta_1 - \beta_2 } < -1$	$\beta_1 - \beta_2 < 0$, $\frac{g_2}{ \beta_1 - \beta_2 } < 0$, $\frac{g_1 - \beta_2 - 0.9g_2}{ \beta_1 - \beta_2 } < -1$ or $\beta_1 - \beta_2 > 0$, $\frac{g_2}{ \beta_1 - \beta_2 } < -1$, $\frac{g_1 - \beta_2 - 0.9g_2}{ \beta_1 - \beta_2 } < -1$	$\beta_1 - \beta_2 < 0$, $\frac{g_2}{ \beta_1 - \beta_2 } > 0$, $\frac{g_1 - \beta_2}{ \beta_1 - \beta_2 } < -1$	$\beta_1 - \beta_2 > 0$, $0 < \frac{g_2}{ \beta_1 - \beta_2 }$, $\frac{g_2}{ \beta_1 - \beta_2 } < 2$, $\frac{g_1 - \beta_2}{ \beta_1 - \beta_2 } < 0$
Fates of magnetic states	✗	✗	✓	✗	✓	✗	✗

crete, we concentrate on a particular point in Fig. 1, namely the QCP at $T = 0$ that separates C_2 and C_4 IC magnetic states labeled by x_c . Generally, the related magnetic fluctuations compete so furiously that are always responsible for physics in the shadow of QPT including quantum critical regime with higher temperatures [14, 22, 23]. Considering that individualities of diverse states, in spite of hosting common magnetic generalities, have different consequences, we thereafter contemplate the magnetic states on both sides of this QPT.

As it concerns the issue on intricate relationship between magnetism and superconductivity, a hallmark of fathoming overall phase diagram is tantamount to pinpointing the specific construction of each magnetic state. As a corollary, it is appropriate that one investigates how the ordering competition affects the magnetic state at the edge of the QCP by means of RG flows (18) in collaboration with the stable magnetic criteria itemized in the second line of Table I.

To proceed, we briefly address our strategy to judge which magnetic candidate is the most stable/favorable state. In principle, there exist two distinct routines to access the QCP as schematically illustrated in Fig. 3. Although the essential physics should be captured by either routine-A or routine-B, we are supposed to witness the physical behaviors along routine-B to examine the stabilities of all potential states. In order to be relevant with the schematic phase diagram, we adopt $T = T_0 e^{-l}$ with

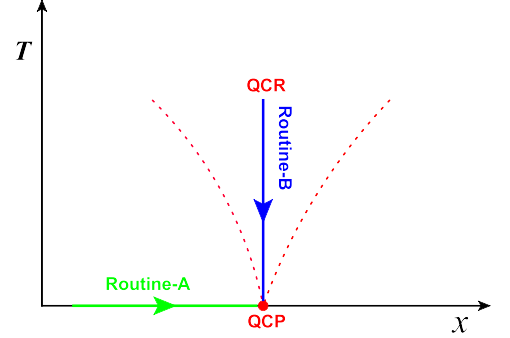


FIG. 3: (Color online) Schematic illustrations for two distinct routines, Routine-A and Routine-B, to access the quantum critical point (QCP) in the $T - x$ plane with T and x corresponding to temperature and non-thermal parameter, respectively. Hereby, QCP and QCR denote the quantum critical point and quantum critical regime [14].

T_0 the initial temperature to measure the evolution variable [18, 31, 35–44]. Subsequently, several procedures are followed to investigate whether a certain SDW state is a suitable candidate. At first, one needs to tune the initial values of fundamental interaction parameters to satisfy the corresponding stable constraint and hence make sure that the starting point (T_0) is located at such SDW state in the quantum critical regime (QCR) of Fig. 3. While we assume the constraint condition is developed in a regime

B. Fates of magnetic states

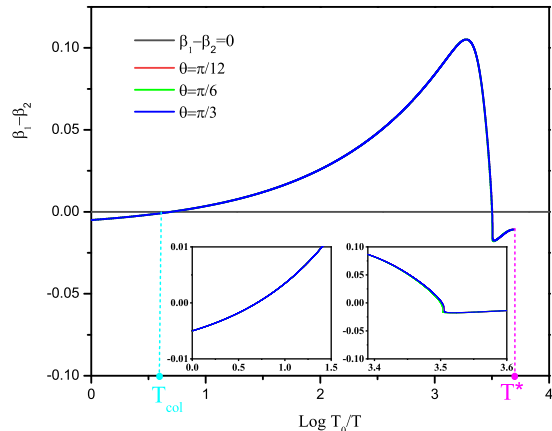


FIG. 4: (Color online) Temperature-dependent stable constraints of the C_2 -symmetry ICS state. Hereby, the angle θ is designated in Sec. II A to specify the direction of magnetic order in the spin space and the initial values of related fundamental parameters are chosen as ($g_1 = 0.01$, $g_2 = 0.01$, $u_s = 0.05$, $\lambda = 0.01$, $\beta_1 = 0.005$, $\beta_2 = 0.01$) for $g_2 > 0$ (the $g_2 < 0$ case exhibits the similar results and hence are not shown) with three representative $\theta = \pi/12, \pi/6, \pi/3$ to satisfy the ICS's stable constraint (the qualitative results are insensitive to initial values of parameters). Apparently, the sign of $\beta_1 - \beta_2$ is changed once temperature is slightly lowered at T_{col} (hereby T_{col} codifies the very temperature at which the ICS stable constrain is jeopardized and collapsed), indicating the violation of the stability constraint which does not make it a good candidate to survive under the strong ordering competition. In addition, the T^* is associated with the underlying fixed point and its related comments are addressed in Sec. III C.

away from the QCP, this SDW state is always stable owing to the absence of quantum fluctuations. In comparison, as approaching the QCP, we have to carefully check whether the stable constraints are still satisfied as the quantum fluctuations become more and more important and play a dominant role in selecting the potential states. To this end, one presents the energy-dependent behaviors of these restrictions after extracting the information from the coupled RG equations of all fundamental interaction parameters (18). With these in hand, it is suitable to determine the stability of such SDW for accessing the QCP. It would be a preferable state once the constraint is well preserved by lowering the energy scale (approaching the QCP). Otherwise, the state is easily melted by ferocious fluctuations and henceforth not a good candidate.

Accordingly, parallelling the similar steps above, we can examine the stabilities of all candidate states one by one on an equal footing and finally select the most favorable SDW states nearby the QCP, which are schematically summarized in Fig. 1 and analyzed in the forthcoming sections.

By employing the strategy in Sec. III A, we within this subsection endeavor to inspect the fates of all magnetic candidate states one by one via performing the RG analysis with respect to the coupled RG evolutions that involve the fluctuations and ordering competitions as well as their interplay.

1. Warm-up

Let us consider the C_2 IC stripe (ICS) magnetic state for an instance and show how to determine whether it is a good candidate (stable/favorable SDW state) for warm-up. The configurations of spin vectors for such state read $\mathbf{n}_X = (0, 0, 1)$ and $\mathbf{n}_Y = (0, 0, 0)$ [19]. As shown in Table I, its stable constraints can be either $(\beta_1 - \beta_2) < 0$, $g_2/|\beta_1 - \beta_2| > 0$, $(g_1 - \beta_2)/|\beta_1 - \beta_2| > -1$ or $(\beta_1 - \beta_2) < 0$, $g_2/|\beta_1 - \beta_2| < 0$, $(g_1 - \beta_2 - 0.9g_2)/|\beta_1 - \beta_2| > -1$ [19]. If this state is favorable around the QCP in the real materials, it must be adequately stable against the quantum fluctuations when approaching the QCP. Accordingly, we can initially choose a higher temperature T_0 away from the QCP as our starting point, at which the initial interaction parameters are supposed to satisfy the stable constraints of C_2 ICS state. Next, we take some representatively initial values of fundamental parameters that obey the stable constraint at T_0 and then perform numerical RG analysis of related RG equations by approaching the QCP along Routine-B as schematically shown in Fig. 3 (namely, by lowering the temperature).

Due to the differences of spin configurations and fluctuations, we recall that all candidate states in Table I possess their own RG equations for the fundamental parameters collected in Appendix A, which dictate the fates of stable constraints of certain states. It is therefore the related RG equations that are in charge of the stability of ICS state when approaching the QCP. After extracting the energy-dependent information from such RG equations, the corresponding numerical results in Fig. 4 display the temperature dependence of flows for the associated fundamental parameters.

In order to compare the robustness with other candidate states, it is helpful to denominate the very temperature as T_{col} at which the candidate state's stable constrain is collapsed. From Fig. 4, we can infer that the sign change of $\beta_1 - \beta_2$ is occurred explicitly once temperature is slightly lowered at $T = T_{\text{col}}$ owing to the effects of ordering competition, hinting at the destruction of the stable constraint. In addition, the basic results are insensitive to the specific values of θ , which are generally rooted in the symmetry of a candidate state [19]. As for the ICS state that does not satisfy the C_4 symmetry, the magnetic components are inequivalent in two directions indicating $\theta \neq \pi/4$, and hence, without loss of generality, three representative values $\theta = \pi/12, \pi/6, \pi/3$ are chosen to perform the numerical calculations. In princi-

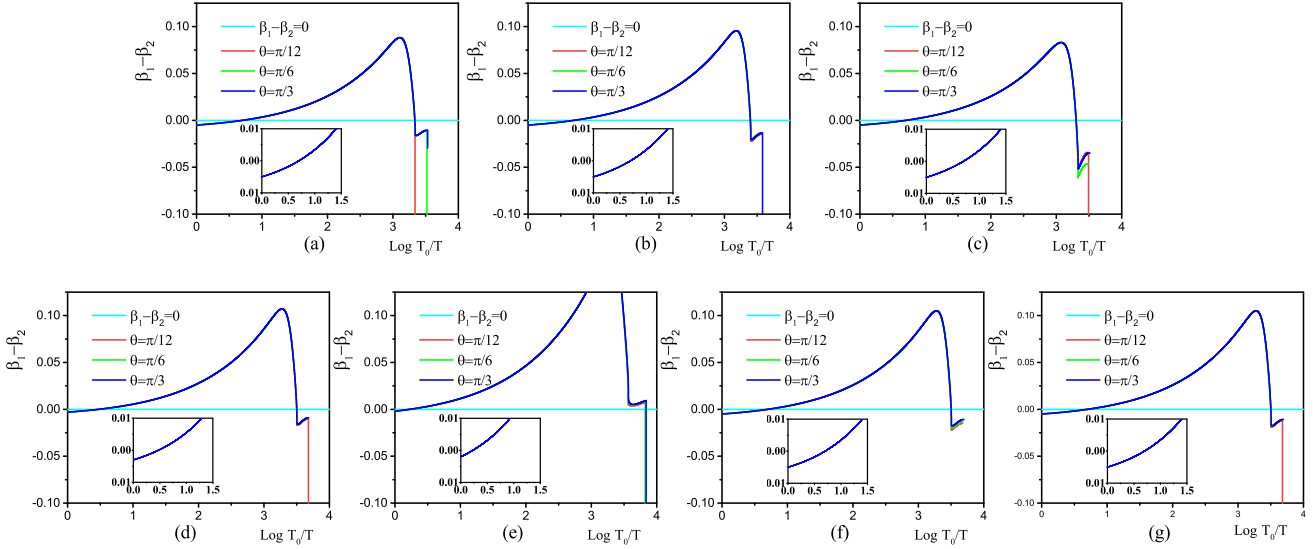


FIG. 5: (Color online) Stability of tendency of temperature-dependence $\beta_1 - \beta_2$ for C_2 ICS magnetic state against adjusting the initial value of Fig. 4: (a) a_s , (b) u_s , (c) λ , (d) β_2 , (e) β_1 , (f) $\lambda_{\Delta A}$, and (g) κ (all cases satisfy the stable constraints of such a state). The angle θ serves as the direction of magnetic order in the spin space and $\theta = \pi/12, \pi/6, \pi/3$ are selected as three representative values. Insets: the sign-change region of $\beta_1 - \beta_2$.

ple, there exists another critical point that describes the fixed point of parameters can be accessed at $l = l^*$ or a related $T = T^*$ beyond which the parameters are divergent or unphysical as labeled in Fig. 4. As presented in Appendix A, different types of candidate SDW states exhibit distinct quantum fluctuations, which give rise to their own sets of RG equations. Henceforth, it is of particular necessity to address that the state with $T < T_{\text{col}}$ is no longer the ICS state but an uncertain state, which possesses unknown but distinct RG equations compared to those of the ICS state. Accordingly, the evolutions of parameters obtained by obeying RG equations of ICS state are unphysical at $T < T_{\text{col}}$ in Fig. 4. This implies that one can neglect the behaviors of parameters at $T < T_{\text{loc}}$ in that whether a candidate state is robust can be determined as T approaches T_{loc} from $T > T_{\text{loc}}$. For convenience, the curves with $T < T_{\text{col}}$ are preserved for comparison with the numerical results of other states.

For completeness, it is worth inspecting whether the fate of an SDW state is robust against the initial fundamental parameters. To this end, we regard the initial condition in Fig. 4 as a reference point and tune an initial parameter of this point but keep all others invariant to form distinct representative groups of initial conditions, all of which are required to meet the stable criteria of C_2 ICS state. The numerical results in Fig. 5 share the similar tendency of $\beta_1 - \beta_2$ to its counterpart in Fig. 4, evincing the robustness of stability against the variation of initial condition. As for all other types of candidates states, the basic results are analogous and thus not shown hereby.

To wrap up, in the spirit of strategy addressed in Sec. III A, we can infer that C_2 ICS is not a stable

state against the quantum fluctuations in the low-energy regime and hence not a good candidate for IC magnetic state nearby the QCP.

2. Stable states

After paralleling the procedures for C_2 ICS state in Sec. III B 1, we check the stabilities of all candidate states collected in Table I. This not only bears witness to the crucial role of ordering competition but also sheds light on fates of all types of IC magnetic states.

To be concrete, Fig. 6 exhibits the temperature (energy) dependence of correlated fundamental parameters, which carry the low-energy characteristics for both C_2 ICS \perp MH and C_4 IC CSDW. At the outset, we find that stable constraints for C_2 ICS \perp MH shown in Fig. 6(a) are well protected with a decrease of temperature. They are sabotaged by extremely strong fluctuations only until the magnetic QCP is sufficiently accessed at the collapsed temperature $T_{\text{col}} \sim 10^{-4}T_0$ (taking $T_0 = 100$ K for instance, $T_{\text{col}} \sim 10^{-2}$ K). This evidently signals that C_2 ICS \perp MH is of particular robustness withstanding ordering competition. In reminiscence of the unknown C_2 magnetic state, which is located at a little deviation from the magnetic QCP portrayed in Fig. 1, we are aware that C_2 ICS \perp MH is therefore deemed to be a reasonable candidate for this mysterious C_2 state that differs substantially from conventional C_2 stripe state. In addition, Fig. 6(b) proposes firmly robust temperature-dependent constraints for C_4 IC CSDW. Moreover, the basic results bearing the similarities to the C_2 ICS presented in Sec. III B 1 are insusceptible to the variances of starting

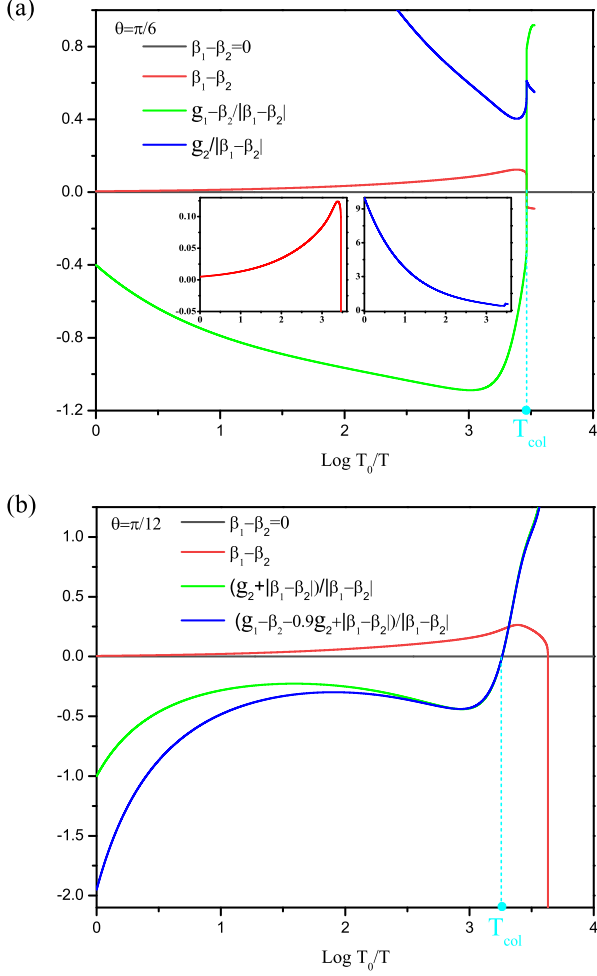


FIG. 6: (Color online) Temperature-dependent stable constraints of (a) C_2 ICS \perp MH and (b) C_4 IC CSDW listed in Table I. Hereby, the angle θ is designated in Sec. II A to specify the direction of magnetic order in the spin space and two representative values $\pi/6$ and $\pi/12$ are selected for cases (a) and (b), respectively. The initial values of related fundamental parameters are chosen as ($g_1 = 0.01$, $g_2 = 0.01$, $u_s = 0.05$, $\lambda = 0.01$, $\beta_1 = 0.01$, $\beta_2 = 0.005$) for ICS \perp MH and ($g_1 = -0.015$, $g_2 = -0.01$, $u_s = 0.05$, $\lambda = 0.01$, $\beta_1 = 0.01$, $\beta_2 = 0.005$) for IC CSDW states (the basic results are insensitive to initial values of parameters). T_{col} labels the very temperature at which the corresponding stable constraints are jeopardized and collapsed. Insets: enlarged regions for $\beta_1 - \beta_2$ and $g_2 / |\beta_1 - \beta_2|$.

parameters as long as they satisfy the restricted conditions listed in Table I (the related further discussions will be briefly delivered in the forthcoming subsection III C).

On the basis of these, we then come to a conclusion that IC CSDW, like its commensurate counterpart [18], behaves dominantly compared to other types of IC C_4 magnetic states. This C_4 magnetic state is hence the most applicable choice on the left side of magnetic QCP x_c in Fig. 1, which compete, coexist, and cooperate with

SC state. Furthermore, apart from the two applicable states including C_2 ICS \perp MH and C_4 IC CSDW, ordering competition surrounded by magnetic QCP is not in favour of all other types of IC magnetic states listed in Table I. In terminological language, given these states are prone to easily feel plus efficiently receive the fluctuation corrections even far away from a magnetic QCP, they are fairly sensitive and fragile to ordering competition, resulting in undeviating breakdown themselves as temperature is reduced. This broadly suggests that one is unable to solely fix the configuration of C_2 IC SDW above C_4 IC CSDW and C_2 ICS \perp MH as displayed in Fig. 1, which may either be C_2 ICS, C_2 DPMH, or C_2 MH. Details of verifying stabilities of IC magnetic states are provided in Appendix B. Last but not the least important, we deliver that, as for the region close enough to the QCP with $T < T_{\text{col}}$, ordering competition is so ferociously that no magnetic state can exist alone but instead there might be a coexistence of multiple IC magnetic states.

C. Relevant comments and explanations

Before going further, we stop to address three relevant issues with comments and explanations.

To begin with, we highlight the major concerns between Ref. [19] and this work are different and then explain the reason for adjusting the initial values not very largely. Concisely, the authors of Ref. [19] focus on how many possible SDW states can be generated and where do they reside in the parameter space via tuning a series of energy-independent parameters. The potential states are separated by several boundaries that are developed by the related parameters and not directly associated with the QCP. In comparison, the phase diagram in Fig. 1 with a QCP is constructed by the temperature and doping, which indicates that the boundaries of these two situations are not the same thing. Additionally, our target is to examine and determine which are the most favorable states among all candidates neighboring the QCP. Following the strategy in Sec. III A, we confine the initial parameters to satisfy the related stable constraints of a candidate state and judge whether such a state is suitable to exist nearby QCP with the help of the corresponding RG equations. In order to make sure the starting point is 100% of the candidate state and avoid the possible influence of other states as different states are associated with different RG equations, it is more suitable to choose the initial parameters a little away from the very boundary of Ref. [19] but near the QCP in Fig. 1. This may be ascribed to a shortage of our strategy in that the RG equations of parameters are based upon the quantum fluctuations around the QCP and we can only deal with the candidate states one by one but cannot tackle two or more mixed states simultaneously.

Afterward, we move on to deliver several comments on the underlying fixed points (FPs) of parameters in

the lowest-energy limit. For convenience, let us suppose that the FPs can be accessed at $T = T^*$, beyond which the parameters are divergent or unphysical as labeled in Fig. 4 for an example. From Fig. 4 or Fig. 6 (whose T^* can be designated analogously to Fig. 4's and have not been shown for brevity), we can infer that the FPs can be accessed either at a much or a little lower energy scale for an unstable ($T^* \ll T_{\text{col}}$) or a stable ($T^* < T_{\text{col}}$) candidate state, implying the parameters do not satisfy the restricted conditions within $T^* < T < T_{\text{col}}$. As a consequence, one can already judge whether some candidate state survives and which are the most favorable states among potential candidates around the QCP before the FPs are exactly approached. Indeed, the FPs may be instructive to other interesting behaviors which are out of scope of our main target and worth systematically studying in future.

Furthermore, it is necessary to present some words on the IC parameter δ in Sec. II A, which does not directly appear in the effective action but is indirectly reflected by imposing the order parameters $M_{\mathbf{Q}_{X,Y}} \neq M_{\mathbf{Q}_{X,Y}}^*$ described in Sec. II A. There exists a little distinction from Puga *et al.*'s pioneering work on the sine-Gordon model [45], in which the parameter δ is explicit in their effective theory. Henceforth, one can regard such parameter as an interaction parameter and examine the transition between a commensurate and an IC state via tracking the evolution of parameter δ . However, all potential states hereby are restricted to IC states and the focus is put on the stability of certain IC state without involving the transition in Ref. [45].

IV. SUPERFLUID DENSITY AND LONDON PENETRATION DEPTH

Generally, the quantum critical region accompanied by a certain QCP is a fertile ground for generating unusual physical behaviors caused by the strong fluctuations, which are of qualitative distinction from the scopes out of control by the QCP. According to Sec. III B 2, the most favorable SDW states for the left and right sides of the QCP correspond to the C_4 IC CSDW and C_2 ICS \perp MH states, respectively. These different sorts of magnetic states would be responsible for distinct fates of physical implications around the QCP. In order to make the logic self-consistent, we follow this clue and endeavor to evaluate the temperature dependence of superfluid density and London penetration depth around both sides of the QCP by taking into account the quantum fluctuations of these two preferable states.

As magnetic states steadily compete and coexist with a SC order, it is of great temptation to examine how the superfluid density (ρ_s) and London penetration depth (λ_L) are influenced in the presence of ordering competition, which has two particularly important implications. In principle, $\rho_s(T)$ can be evaluated as $\rho_s(T) = \rho_s^A(T) -$

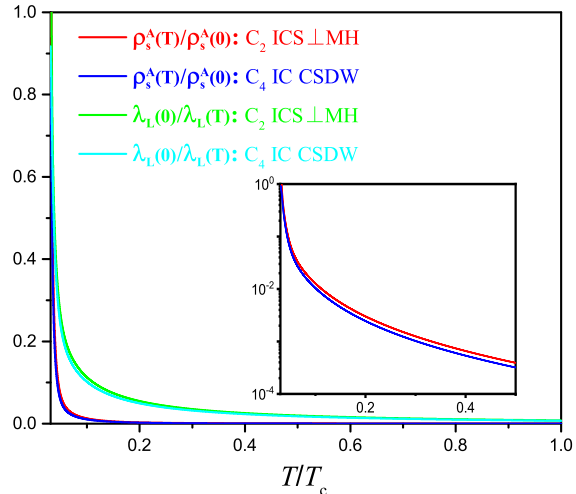


FIG. 7: (Color online) Superfluid density and London penetration depth as a function of temperature at $\theta = 6/\pi$ affected by C_2 ICS \perp MH and C_4 IC CSDW states neighboring the magnetic QCP. Hereby, T_c designates the related critical temperature without the ordering competition and the angle θ characterizes the direction of magnetic order in the spin space, which is assigned a representative value ($\pi/6$) for numerical evaluation (the essential features are insensitive to beginning values of interaction parameters and concrete directions of such magnetic order). Inset: enlarged regions for ρ_s displaying difference between the two cases.

$\rho_n(T)$, where $\rho_s^A(T) \propto \alpha_A(T)$ stems from the mass of vector field \mathbf{A} that obey RG equations due to Anderson-Higgs mechanism [29] and $\rho_n(T)$ grasps the density of thermally excited normal (non-SC) fermionic quasiparticles (QPs), respectively. Approaching the QCP, ordering competition is dominant and thus the normal QPs effects can be neglected implying $\rho_s(T) \sim \rho_s^A(T)$.

Fig. 7 clearly shows that $\rho_s(T)$ is notably suppressed by the ordering competition [18, 46, 47]. Because critical temperature T_c is nominated by $\rho_s(T_c) = \rho_s^A(T) - \rho_n(T) = 0$, one can infer that it would be intensively reduced in the absence of $\rho_n(T)$. As explicitly delineated in the inset of Fig. 7, it is worth declaring that the drop of T_c caused by the C_4 IC CSDW is a little more than its C_2 ICS \perp MH's counterpart, which is also apparently exposed in Fig. 1. Albeit a slight splitting, principal tendencies are qualitatively compatible with recent experiments [6, 8, 10]. As for the unconventional derivation of temperature-dependent ρ_s from usual s -wave gap symmetry's, there are two underlying reasons. A major concern is the possible alteration of the pairing gap symmetry driven by so ferocious fluctuations around the QCP. In addition, the fundamental interaction parameters can also display anomalous energy-dependence behaviors as accessing the QCP, which enter into the analytical expression of ρ_s and hence can indirectly influence the tendency of superfluid.

For qualitative discussions, we single out the s -wave gap symmetry as a toy and tentative substitute. In this respect, the London penetration depth is expressed as $\lambda_L(0)/\lambda_L(T) = \sqrt{\rho_s(T)}$ [48]. As a consequence, $\lambda_L(0)/\lambda_L(T)$ shares an analogous temperature-dependent trajectory with ρ_s under the impact of ordering competition as depicted in Fig. 7. Although BaFe_2As_2 system possesses a more intricate gap structure [13], this primitive result might uncover parts of central ingredients that are in charge of λ_L 's property. For completeness, we adopt the method in Sec. III B 2 and check that the basic conclusions concerning the superfluid density in Fig. 7 are robust under the variation of couplings between SDW and SC, which are embodied by the initial fundamental parameters.

As a consequence, the behaviors of physical observables indirectly corroborate C_4 IC CSDW and C_2 ICS \perp MH states are favorable SDW states compared to the other candidates in Table I. This implies that the phenomenological theory can qualitatively capture the key information around the QCP. In addition, the primary conclusions concerning the preferable SDW states neighboring the putative QCP are relatively stable and self-consistent.

V. SUMMARY

To recapitulate, we study and discern the probable IC magnetic states induced by subtle ordering competition in the proximity of certain QPT below the SC dome of $\text{Ba}_{1-x}\text{Na}_x\text{Fe}_2\text{As}_2$. Specifically, we find that C_2 ICS \perp MH survives to be a good candidate for the obscure C_2 magnetic state and IC C_4 CSDW points to the reasonable IC state in the vicinity of the magnetic QPT. In addition, we address that superfluid density in tandem with critical temperature and London penetration depth manifest critical behaviors attesting to ordering competition around the QCP.

Fig. 1 schematically presents our primary conclusions, whose overall structure is borrowed from the experimental results in Ref. [8]. However, it is worth pointing out that the spin configurations of magnetic states for both sides of the QCP are unclear and hence only labeled by SDW state in Wang *et al.*'s work [8]. In sharp contrast, we explicitly determine that the most favorable candidates for the left and right sides correspond to the C_4 IC CSDW and C_2 ICS \perp MH states by virtue of one-loop RG analysis. In addition, we theoretically address that the C_4 IC CSDW state is more harmful to the superconductivity. The conclusions are qualitatively concomitant with recent experiments [6, 8, 10]. In this sense, we offer a relatively operable strategy to select out the most favorable states around the QCP, with which one can in principle

examine whether some magnetic state is a preferable state against the influence of quantum fluctuations. We expect our results are profitable to further understand the phase diagram of $\text{Ba}_{1-x}\text{Na}_x\text{Fe}_2\text{As}_2$ and explore the correspondence between SC and magnetic states in the iron-based superconductors.

ACKNOWLEDGEMENTS

J.W. is partially supported by the National Natural Science Foundation of China under Grant No. 11504360 and highly grateful to Ya-Jie Zhou for stimulating discussions on the June 11, 2020. The author also acknowledges the Referee A from PRL for the constructive comments and suggestions.

Appendix A: Coupled RG equations of fundamental interaction parameters

After performing one-loop analysis of effective theory [18, 20, 31] via integrating out the fields in the momentum shell $e^{-l}\Lambda < k < \Lambda$ with $l > 0$ the running scale, we can derive flows of effective parameters in Eq. (8). Combining these equations and connections (9)-(17) [18, 31], the coupled RG equations for fundamental parameters can be derived.

Before going further, it is necessary to highlight that the fundamental parameters $g_{1,2}$ only appear in Eq. (15). This implies that they do not evolve independently. In this sense, it is hereafter convenient to introduce a parameter

$$\hat{g} \equiv g_1 \cos^2 \theta \sin^2 \theta (|\mathbf{n}_X|^2 |\mathbf{n}_Y|^2) + \frac{g_2}{2} \cos^2 \theta \sin^2 \theta (|\mathbf{n}_X \cdot \mathbf{n}_Y|^2 + |\mathbf{n}_X \cdot \mathbf{n}_Y^*|^2), \quad (\text{A1})$$

to describe the information of $g_{1,2}$.

After long but straightforward calculations [18, 31], we eventually obtain the coupled RG equations of all fundamental interaction parameters around the magnetic QCP, which include $\alpha, \beta_{1,2}, \hat{g}$ and κ specifying the characters of spin configurations as well as $a_s, u_s, \lambda_{\Delta A}$ stemming from SC fluctuations. These coupled RG evolutions are closely dependent upon the spin configurations of magnetic fluctuations, namely the relationships between $|\mathbf{n}_X^2|^2, |\mathbf{n}_X|^4, |\mathbf{n}_Y^2|^2, |\mathbf{n}_Y|^4$, which are divided into two main sorts of situations.

For type-I case, at which $|\mathbf{n}_X^2|^2 \neq |\mathbf{n}_X|^4$ and $|\mathbf{n}_Y^2|^2 = |\mathbf{n}_Y|^4$ or $|\mathbf{n}_X^2|^2 = |\mathbf{n}_X|^4$ and $|\mathbf{n}_Y^2|^2 \neq |\mathbf{n}_Y|^4$, both β_1 and β_2 flow independently and thus the coupled evolutions are written as

$$\begin{aligned} \frac{da_s}{dl} = & 2a_s - \frac{1}{4\pi^2} \left\{ \frac{9a_s u_s (1 + 4a_s)}{2} + \frac{2\mathcal{S}\mathcal{E}_1^2 a_s \lambda^2}{u_s} [1 - 4\mathcal{S}\mathcal{E}_1(a - \frac{\lambda a_s}{u_s})] + \frac{2\mathcal{C}\mathcal{D}_1^2 a_s \lambda^2}{u_s} [1 - 4\mathcal{C}\mathcal{D}_1(a - \frac{\lambda a_s}{u_s})] \right. \\ & + \frac{32a_s \lambda_{\Delta A}^2}{3u_s} (1 + \frac{4\lambda_{\Delta A} a_s}{u_s}) + \frac{(\mathcal{S}\mathcal{E}_1 + \mathcal{C}\mathcal{D}_1)\lambda}{2} + \frac{3u_s(1 + 2a_s)}{4} - (a - \frac{\lambda a_s}{u_s})(\mathcal{E}_1^2 \mathcal{S}^2 + \mathcal{D}_1^2 \mathcal{C}^2)\lambda \\ & \left. + \lambda_{\Delta A}(1 + \frac{2\lambda_{\Delta A} a_s}{u_s}) + \frac{\mathcal{C}\mathcal{S}\mathcal{F}^2 a_s \kappa^2}{4u_s} [1 - 2(\mathcal{C}\mathcal{D}_1 + \mathcal{S}\mathcal{E}_1)(a - \frac{\lambda a_s}{u_s})] \right\}, \end{aligned} \quad (\text{A2})$$

$$\begin{aligned} \frac{da}{dl} = & 2(a - \frac{\lambda a_s}{u_s}) + \frac{1}{4\pi^2} \left\{ \frac{\lambda}{2} + \frac{\mathcal{S}\hat{g}}{\mathcal{D}_1} + 3\mathcal{C}[\beta_2 \mathcal{D}_1 + (\beta_1 - \beta_2) \frac{\mathcal{D}_2}{\mathcal{D}_1}] - \frac{2\mathcal{S}^2 \mathcal{E}_1 \hat{g}}{\mathcal{D}_1} (a - \frac{\lambda a_s}{u_s}) \right. \\ & - 6\mathcal{C}^2(a - \frac{\lambda a_s}{u_s})[\beta_2 \mathcal{D}_1^2 + (\beta_1 - \beta_2) \mathcal{D}_2] + a_s \lambda + \frac{4\mathcal{C}\mathcal{D}_1 a_s \lambda^2}{u_s} [1 - 2(\mathcal{C}\mathcal{D}_1(a - \frac{\lambda a_s}{u_s}) - a_s)] \\ & \left. - \frac{\mathcal{S}\mathcal{F}^2 \kappa^2}{8\mathcal{D}_1} [1 - 2(\mathcal{S}\mathcal{E}_1(a - \frac{\lambda a_s}{u_s}) - a_s)] \right\} + \left(\frac{\lambda}{u_s} \frac{da_s}{dl} + \frac{a_s}{u_s} \frac{d\lambda}{dl} - \frac{a_s \lambda}{u_s^2} \frac{du_s}{dl} \right), \end{aligned} \quad (\text{A3})$$

$$\begin{aligned} \frac{du_s}{dl} = & u_s + \frac{1}{2\pi^2} \left\{ -18a_s u_s^2 (1 + 6a_s) - \frac{16\mathcal{C}^3 \mathcal{D}_1^3 a_s \lambda^3}{3u_s} [1 - 6\mathcal{C}(a - \frac{\lambda a_s}{u_s}) \mathcal{D}_1] - \frac{16\mathcal{S}^3 \mathcal{E}_1^3 a_s \lambda^3}{3u_s} [1 - 6\mathcal{S}(a - \frac{\lambda a_s}{u_s}) \mathcal{E}_1] \right. \\ & + 8\lambda^2 (\mathcal{S}^3 \mathcal{E}_1^3 + \mathcal{C}^3 \mathcal{D}_1^3) (a - \frac{\lambda a_s}{u_s}) - 18a_s u_s^2 - \frac{9u_s^2}{2} - 2\lambda^2 (\mathcal{S}^2 \mathcal{E}_1^2 + \mathcal{C}^2 \mathcal{D}_1^2) - \frac{32\lambda_{\Delta A}^2}{3} (\frac{4\lambda_{\Delta A} a_s}{u_s} + 1) \\ & - \frac{11072a_s \lambda_{\Delta A}^3}{105u_s} (1 + \frac{6\lambda_{\Delta A} a_s}{u_s}) - \mathcal{C}\mathcal{S}\mathcal{F}^2 \kappa^2 [1 - 2(\mathcal{C}\mathcal{D}_1 + \mathcal{S}\mathcal{E}_1)(a - \frac{\lambda a_s}{u_s})] \\ & - \frac{\mathcal{C}^2 \mathcal{S}^2 \mathcal{F}^2 a_s^2 \kappa^2 (\mathcal{F}^2 \kappa^2 + 2\mathcal{D}_1 \mathcal{E}_1 \lambda^2)}{6u_s^2} [1 - 4(\mathcal{C}\mathcal{D}_1 + \mathcal{S}\mathcal{E}_1)(a - \frac{\lambda a_s}{u_s})] \\ & \left. - \frac{2\mathcal{C}^2 \mathcal{S}\mathcal{F}^2 \mathcal{D}_1 a_s \kappa^2 \lambda}{3u_s} [1 - 2(2\mathcal{C}\mathcal{D}_1 + \mathcal{S}\mathcal{E}_1)(a - \frac{\lambda a_s}{u_s})] \right\}, \end{aligned} \quad (\text{A4})$$

$$\begin{aligned} \frac{d\lambda}{dl} = & \lambda + \frac{1}{2\pi^2} \left\{ \frac{-8\mathcal{S}^3 \mathcal{E}_1^2 a_s \lambda^2 \hat{g}}{3\mathcal{D}_1 u_s} [1 - 6\mathcal{S}\mathcal{E}_1(a - \frac{\lambda a_s}{u_s})] - \frac{8\mathcal{C}^3 \mathcal{D}_1 a_s \lambda^2 [\beta_2 \mathcal{D}_1^2 + (\beta_1 - \beta_2) \mathcal{D}_2]}{u_s} \right. \\ & \times [1 - 6\mathcal{C}\mathcal{D}_1(a - \frac{\lambda a_s}{u_s})] - 4\mathcal{C}\mathcal{D}_1 a_s \lambda^2 [1 - 2(\mathcal{C}\mathcal{D}_1(a - \frac{\lambda a_s}{u_s}) - 2a_s)] - \frac{8\mathcal{C}^2 \mathcal{D}_1^2 a_s \lambda^3}{3u_s} [1 - 2(2\mathcal{C}\mathcal{D}_1(a - \frac{\lambda a_s}{u_s}) - a_s)] \\ & + 3a_s u_s \lambda (1 + 6a_s) - \frac{\mathcal{S}\mathcal{F}^2 \kappa^2}{\mathcal{D}_1} [1 - 2(\mathcal{S}\mathcal{E}_1(a - \frac{\lambda a_s}{u_s}) - a_s)] + \frac{\mathcal{S}^2 \mathcal{E}_1 \lambda \hat{g}}{\mathcal{D}_1} [4\mathcal{S}\mathcal{E}_1(a - \frac{\lambda a_s}{u_s}) - 1] \\ & - \frac{3u_s(1 + 4a_s)\lambda}{4} + 3\mathcal{C}^2 \lambda [\beta_2 \mathcal{D}_1^2 + (\beta_1 - \beta_2) \mathcal{D}_2] [4\mathcal{C}\mathcal{D}_1(a - \frac{\lambda a_s}{u_s}) - 1] + 4\mathcal{C}\mathcal{D}_1 \lambda^2 [2(\mathcal{C}\mathcal{D}_1(a - \frac{\lambda a_s}{u_s}) - a_s) - 1] \\ & - \frac{2\mathcal{S}^2 \mathcal{F}^2 \mathcal{E}_1 \lambda a_s \kappa^2}{3\mathcal{D}_1 u_s} [1 - 2(2\mathcal{S}\mathcal{E}_1(a - \frac{\lambda a_s}{u_s}) - a_s)] - \frac{2\mathcal{C}\mathcal{S}\mathcal{F}^2 a_s \lambda \kappa^2}{3u_s} [1 - 2(\mathcal{C}\mathcal{D}_1 + \mathcal{S}\mathcal{E}_1)(a - \frac{\lambda a_s}{u_s}) + 2a_s] \\ & - \frac{\mathcal{C}^2 \mathcal{S}^2 \mathcal{E}_1 \mathcal{F}^2 \lambda a_s^2 \kappa^2 [\beta_2 \mathcal{D}_1^2 + (\beta_1 - \beta_2) \mathcal{D}_2]}{2\mathcal{D}_1 u_s^2} [1 - 4(\mathcal{C}\mathcal{D}_1(a - \frac{\lambda a_s}{u_s}) + \mathcal{S}\mathcal{E}_1(a - \frac{\lambda a_s}{u_s}))] \\ & \left. - \frac{\mathcal{C}^2 \mathcal{S}^2 \mathcal{F}^2 \lambda a_s^2 \kappa^2 \hat{g}}{6u_s^2} [1 - 4(\mathcal{C}\mathcal{D}_1 + \mathcal{S}\mathcal{E}_1)(a - \frac{\lambda a_s}{u_s})] \right\}, \end{aligned} \quad (\text{A5})$$

$$\begin{aligned} \frac{d\beta_1}{dl} = & \frac{[(\mathcal{D}_1^2 - \mathcal{D}_2) \mathcal{E}_2 - (\mathcal{E}_1^2 - \mathcal{E}_2) \mathcal{D}_2]}{(\mathcal{D}_1^2 \mathcal{E}_2 - \mathcal{E}_1^2 \mathcal{D}_2)} \beta_1 + \frac{2(\mathcal{D}_1^2 - \mathcal{D}_2)}{2\pi^2 (\mathcal{D}_1^2 \mathcal{E}_2 - \mathcal{E}_1^2 \mathcal{D}_2)} \left\{ \mathcal{C}^2 \hat{g}^2 [4\mathcal{C}\mathcal{D}_1(a - \frac{\lambda a_s}{u_s}) - 1] \right. \\ & - \frac{\mathcal{E}_1^2 \lambda^2 (1 + 4a_s)}{4} - 9\mathcal{S}^2 [\beta_2 \mathcal{E}_1^2 + (\beta_1 - \beta_2) \mathcal{E}_2]^2 [1 - 4\mathcal{S}\mathcal{E}_1(a - \frac{\lambda a_s}{u_s})] - \frac{4\mathcal{S}^2 \mathcal{E}_1^2 a_s \lambda^2 [\beta_2 \mathcal{E}_1^2 + (\beta_1 - \beta_2) \mathcal{E}_2]}{u_s} \\ & \times [1 - 2(2\mathcal{S}\mathcal{E}_1(a - \frac{\lambda a_s}{u_s}) - a_s)] - \frac{4\mathcal{S}\mathcal{E}_1^3 a_s \lambda^3}{3u_s} [1 - 2(\mathcal{S}\mathcal{E}_1(a - \frac{\lambda a_s}{u_s}) - 2a_s)] - \frac{2\mathcal{C}^2 \mathcal{F}^2 a_s \kappa^2 \hat{g}}{3u_s} \\ & \times [1 - 2(2\mathcal{C}\mathcal{D}_1(a - \frac{\lambda a_s}{u_s}) - a_s)] \left. \right\} - \frac{2(\mathcal{E}_1^2 - \mathcal{E}_2)}{2\pi^2 (\mathcal{D}_1^2 \mathcal{E}_2 - \mathcal{E}_1^2 \mathcal{D}_2)} \left\{ \frac{-4\mathcal{C}^2 \mathcal{D}_1^2 a_s \lambda^2 [\beta_2 \mathcal{D}_1^2 + (\beta_1 - \beta_2) \mathcal{D}_2]}{u_s} \right. \\ & \times [1 - 2(2\mathcal{C}\mathcal{D}_1(a - \frac{\lambda a_s}{u_s}) - a_s)] + 9\mathcal{C}^2 [\beta_2 \mathcal{D}_1^2 + (\beta_1 - \beta_2) \mathcal{D}_2]^2 [4\mathcal{C}\mathcal{D}_1(a - \frac{\lambda a_s}{u_s}) - 1] \\ & + \mathcal{S}^2 \hat{g}^2 [4\mathcal{S}\mathcal{E}_1(a - \frac{\lambda a_s}{u_s}) - 1] - \frac{\mathcal{D}_1^2 \lambda^2 (1 + 4a_s)}{4} - \frac{4\mathcal{C}\mathcal{D}_1^3 a_s \lambda^3}{3u_s} [1 - 2(\mathcal{C}\mathcal{D}_1(a - \frac{\lambda a_s}{u_s}) - 2a_s)] \\ & \left. - \frac{2\mathcal{S}^2 \mathcal{F}^2 a_s \kappa^2 \hat{g}}{3u_s} [1 - 2(2\mathcal{S}\mathcal{E}_1(a - \frac{\lambda a_s}{u_s}) - a_s)] \right\}, \end{aligned} \quad (\text{A6})$$

$$\frac{d\beta_2}{dl} = \frac{(\mathcal{E}_2 \mathcal{D}_1^2 - \mathcal{D}_2 \mathcal{E}_1^2)}{(\mathcal{D}_1^2 \mathcal{E}_2 - \mathcal{E}_1^2 \mathcal{D}_2)} \beta_2 + \frac{2\mathcal{E}_2}{2\pi^2 (\mathcal{D}_1^2 \mathcal{E}_2 - \mathcal{E}_1^2 \mathcal{D}_2)} \left\{ \mathcal{S}^2 \hat{g}^2 [4\mathcal{S}\mathcal{E}_1(a - \frac{\lambda a_s}{u_s}) - 1] - \frac{\mathcal{D}_1^2 \lambda^2 (1 + 4a_s)}{4} \right\}$$

$$\begin{aligned}
& +9\mathcal{C}^2[\beta_2\mathcal{D}_1^2 + (\beta_1 - \beta_2)\mathcal{D}_2]^2[4\mathcal{C}\mathcal{D}_1(a - \frac{\lambda a_s}{u_s}) - 1] - \frac{4\mathcal{C}^2\mathcal{D}_1^2 a_s \lambda^2 [\beta_2\mathcal{D}_1^2 + (\beta_1 - \beta_2)\mathcal{D}_2]}{u_s} \\
& \times [1 - 2(\mathcal{C}\mathcal{D}_1(a - \frac{\lambda a_s}{u_s}) - a_s)] - \frac{4\mathcal{C}^3\mathcal{D}_1^3 a_s \lambda^3}{3u_s} [1 - 2(\mathcal{C}\mathcal{D}_1(a - \frac{\lambda a_s}{u_s}) - 2a_s)] - \frac{2\mathcal{S}^2\mathcal{F}^2 a_s \kappa^2 \hat{g}}{3u_s} \\
& \times [1 - 2(2\mathcal{S}\mathcal{E}_1(a - \frac{\lambda a_s}{u_s}) - a_s)] \Big\} - \frac{2\mathcal{D}_2}{2\pi^2(\mathcal{D}_1^2\mathcal{E}_2 - \mathcal{E}_1^2\mathcal{D}_2)} \Big\{ \frac{-4\mathcal{S}^2\mathcal{E}_1^2 a_s \lambda^2 [\beta_2\mathcal{E}_1^2 + (\beta_1 - \beta_2)\mathcal{E}_2]}{u_s} \\
& \times [1 - 2(2\mathcal{S}\mathcal{E}_1(a - \frac{\lambda a_s}{u_s}) - a_s)] - 9\mathcal{S}^2[\beta_2\mathcal{E}_1^2 + (\beta_1 - \beta_2)\mathcal{E}_2]^2 [1 - 4\mathcal{S}\mathcal{E}_1(a - \frac{\lambda a_s}{u_s})] + \mathcal{C}^2\hat{g}^2 \\
& \times [4\mathcal{C}\mathcal{D}_1(a - \frac{\lambda a_s}{u_s}) - 1] - \frac{\mathcal{E}_1^2\lambda^2(1 + 4a_s)}{4} + \frac{-4\mathcal{S}\mathcal{E}_1^3 a_s \lambda^3}{3u_s} [1 - 2(\mathcal{S}\mathcal{E}_1(a - \frac{\lambda a_s}{u_s}) - 2a_s)] \\
& + \frac{-2\mathcal{C}^2\mathcal{F}^2 a_s \kappa^2 \hat{g}}{3u_s} [1 - 2(\mathcal{C}\mathcal{D}_1(a - \frac{\lambda a_s}{u_s}) - a_s)] \Big\}, \tag{A7}
\end{aligned}$$

$$\begin{aligned}
\frac{d\lambda_{\Delta A}}{dl} = & \lambda_{\Delta A} + \frac{2}{2\pi^2} \Big\{ \frac{-64a_s\lambda_{\Delta A}^3}{9u_s} [1 - 2(\mathcal{D}_1(a - \frac{\lambda a_s}{u_s}) - a_s)] - \frac{3a_s u_s \lambda_{\Delta A} (1 + 6a_s)}{2} - \frac{3u_s \lambda_{\Delta A} (4a_s + 1)}{8} \\
& - 4\lambda_{\Delta A}^2 [1 + 2a_s(1 + \frac{\lambda_{\Delta A}}{u_s})] - 4a_s \lambda_{\Delta A}^2 [1 + (4a_s + \frac{2\lambda_{\Delta A} a_s}{u_s})] \Big\}, \tag{A8}
\end{aligned}$$

$$\begin{aligned}
\frac{d\kappa}{dl} = & \kappa + \frac{2}{2\pi^2} \Big\{ \frac{-2\mathcal{C}\mathcal{S}\mathcal{D}_1\mathcal{E}_1 a_s \lambda^2 \kappa}{3u_s} [1 - 2(\mathcal{C}\mathcal{D}_1(a - \frac{\lambda a_s}{u_s}) + \mathcal{S}\mathcal{E}_1(a - \frac{\lambda a_s}{u_s}) - a_s)] - \frac{3a_s u_s \kappa (1 + 6a_s)}{2} \\
& - \mathcal{C}\mathcal{S}\hat{g}\kappa [1 - 2(\mathcal{C}\mathcal{D}_1(a - \frac{\lambda a_s}{u_s}) + \mathcal{S}\mathcal{E}_1(a - \frac{\lambda a_s}{u_s}))] - \frac{3(1 + 4a_s)u_s \kappa}{8} - \frac{2\mathcal{C}\mathcal{S}^2\mathcal{E}_1\hat{g}a_s \kappa \lambda}{3u_s} \\
& \times [1 - 2(\mathcal{C}\mathcal{D}_1(a - \frac{\lambda a_s}{u_s}) + 2\mathcal{S}\mathcal{E}_1(a - \frac{\lambda a_s}{u_s}))] - \frac{\mathcal{C}^2\mathcal{S}^2\mathcal{F}^2\hat{g}a_s^2 \kappa^3}{6u_s^2} [1 - 4(\mathcal{C}\mathcal{D}_1(a - \frac{\lambda a_s}{u_s}) + \mathcal{S}\mathcal{E}_1(a - \frac{\lambda a_s}{u_s}))] \\
& - \frac{2\mathcal{C}^2\mathcal{S}\mathcal{D}_1\hat{g}a_s \kappa \lambda}{3u_s} [1 - 2(2\mathcal{C}\mathcal{D}_1(a - \frac{\lambda a_s}{u_s}) + \mathcal{S}\mathcal{E}_1(a - \frac{\lambda a_s}{u_s}))] \Big\}, \tag{A9}
\end{aligned}$$

$$\begin{aligned}
\frac{d\hat{g}}{dl} = & \hat{g} + \frac{1}{2\pi^2} \Big\{ \frac{-4\mathcal{C}\mathcal{D}_1^2\mathcal{E}_1 a_s \lambda^3}{3u_s} [1 - 2(\mathcal{C}\mathcal{D}_1(a - \frac{\lambda a_s}{u_s}) - 2a_s)] + \frac{-4\mathcal{S}\mathcal{D}_1\mathcal{E}_1^2 a_s \lambda^3}{3u_s} [1 - 2(\mathcal{S}\mathcal{E}_1(a - \frac{\lambda a_s}{u_s}) - 2a_s)] \\
& - \frac{32\mathcal{C}^2\mathcal{D}_1^2\hat{g}a_s \lambda^2}{3u_s} [1 - 2(2\mathcal{C}\mathcal{D}_1(a - \frac{\lambda a_s}{u_s}) - a_s)] + \mathcal{S}^3\mathcal{E}_1(a - \frac{\lambda a_s}{u_s})[\beta_2\mathcal{E}_1^2 + (\beta_1 - \beta_2)\mathcal{E}_2] \\
& - \frac{32\mathcal{S}^2\mathcal{E}_1^2\hat{g}a_s \lambda^2}{3u_s} [1 - 2(2\mathcal{S}\mathcal{E}_1(a - \frac{\lambda a_s}{u_s}) - a_s)] - \frac{\mathcal{F}^2(1 + 4a_s)\kappa^2}{4} - \frac{\mathcal{D}_1\mathcal{E}_1(4a_s + 1)\lambda^2}{4} \\
& + 12\hat{g}[\mathcal{C}^3\mathcal{D}_1(a - \frac{\lambda a_s}{u_s})[\beta_2\mathcal{D}_1^2 + (\beta_1 - \beta_2)\mathcal{D}_2] + 8\mathcal{C}\mathcal{S}\hat{g}^2[2(\mathcal{C}\mathcal{D}_1(a - \frac{\lambda a_s}{u_s}) \\
& + \mathcal{S}\mathcal{E}_1(a - \frac{\lambda a_s}{u_s})) - 1] - 3(\hat{g} - \beta_2\mathcal{D}_1\mathcal{E}_1)[\mathcal{C}^2[\beta_2\mathcal{D}_1^2 + (\beta_1 - \beta_2)\mathcal{D}_2] + \mathcal{S}^2[\beta_2\mathcal{E}_1^2 + (\beta_1 - \beta_2)\mathcal{E}_2]] \\
& - \frac{2\mathcal{C}^2\mathcal{F}^2[\beta_2\mathcal{D}_1^2 + (\beta_1 - \beta_2)\mathcal{D}_2]a_s \kappa^2}{u_s} [1 - 2(2\mathcal{C}\mathcal{D}_1(a - \frac{\lambda a_s}{u_s}) - a_s)] - \frac{2\mathcal{S}^2\mathcal{F}^2[\beta_2\mathcal{E}_1^2 + (\beta_1 - \beta_2)\mathcal{E}_2]a_s \kappa^2}{u_s} \\
& \times [1 - 2(2\mathcal{S}\mathcal{E}_1(a - \frac{\lambda a_s}{u_s}) - a_s)] - \frac{4\mathcal{C}^2\mathcal{S}^2\mathcal{F}^2\hat{g}^2 a_s^2 \kappa^2}{3u_s^2} [1 - 4(\mathcal{C}\mathcal{D}_1(a - \frac{\lambda a_s}{u_s}) + \mathcal{S}\mathcal{E}_1(a - \frac{\lambda a_s}{u_s}))] \\
& - \frac{3\mathcal{C}^2\mathcal{S}^2\mathcal{F}^2[\beta_2\mathcal{D}_1^2 + (\beta_1 - \beta_2)\mathcal{D}_2][\beta_2\mathcal{E}_1^2 + (\beta_1 - \beta_2)\mathcal{E}_2]a_s^2 \kappa^2}{2u_s^2} [1 - 4(\mathcal{C}\mathcal{D}_1(a - \frac{\lambda a_s}{u_s}) + \mathcal{S}\mathcal{E}_1(a - \frac{\lambda a_s}{u_s}))] \\
& - \frac{\mathcal{C}^2\mathcal{S}^2\mathcal{F}^2\hat{g}^2 a_s^2 \kappa^2}{3u_s^2} [1 - 4(\mathcal{C}\mathcal{D}_1(a - \frac{\lambda a_s}{u_s}) + \mathcal{S}\mathcal{E}_1(a - \frac{\lambda a_s}{u_s}))] \Big\}, \tag{A10}
\end{aligned}$$

where the variable functions are designated as

$$\mathcal{D}_1 \equiv |\mathbf{n}_X|^2 \cos^2 \theta, \quad \mathcal{D}_2 \equiv |\mathbf{n}_X^2|^2 \cos^4 \theta, \quad \mathcal{E}_1 \equiv |\mathbf{n}_Y|^2 \sin^2 \theta, \quad \mathcal{E}_2 \equiv |\mathbf{n}_Y^2|^2 \sin^4 \theta, \tag{A11}$$

$$\mathcal{F} \equiv |\cos \theta \sin \theta \mathbf{n}_X \cdot \mathbf{n}_Y| + |\cos \theta \sin \theta \mathbf{n}_X \cdot \mathbf{n}_Y^*|, \quad \mathcal{C} \equiv 1/|\mathbf{n}_X \cos \theta|^2, \quad \mathcal{S} \equiv 1/|\mathbf{n}_Y \sin \theta|^2. \tag{A12}$$

Here, we would like to stress that $\theta \in [0, \pi/2]$, and $\theta = 0, \pi/2$ serve as single magnetic order parameter with \mathbf{Q}_X or \mathbf{Q}_Y , respectively.

For type-II case, at which $|\mathbf{n}_i^2|^2 \neq |\mathbf{n}_i|^4$ with $i = X, Y$, only one of β_1 and β_2 flows independently. In this circumstance, the flows of a_s , a , u_s , λ , $\lambda_{\Delta A}$ and κ share the same evolutions with their type-I counterparts. Nevertheless, the parameter \hat{g} evolves under the following way

$$\begin{aligned}
\frac{d\hat{g}}{dl} = & \hat{g} + \frac{1}{2\pi^2} \Big\{ \frac{-4\mathcal{C}\mathcal{D}_1^2\mathcal{E}_1 a_s \lambda^3}{3u_s} [1 - 2(\mathcal{C}\mathcal{D}_1(a - \frac{\lambda a_s}{u_s}) - 2a_s)] - \frac{4\mathcal{S}\mathcal{D}_1\mathcal{E}_1^2 a_s \lambda^3}{3u_s} [1 - 2(\mathcal{S}\mathcal{E}_1(a - \frac{\lambda a_s}{u_s}) - 2a_s)] \\
& - \frac{32\mathcal{C}^2\mathcal{D}_1^2\hat{g}a_s \lambda^2}{3u_s} [1 - 2(2\mathcal{C}\mathcal{D}_1(a - \frac{\lambda a_s}{u_s}) - a_s)] - \frac{32\mathcal{S}^2\mathcal{E}_1^2\hat{g}a_s \lambda^2}{3u_s} [1 - 2(2\mathcal{S}\mathcal{E}_1(a - \frac{\lambda a_s}{u_s}) - a_s)] \Big\}
\end{aligned}$$

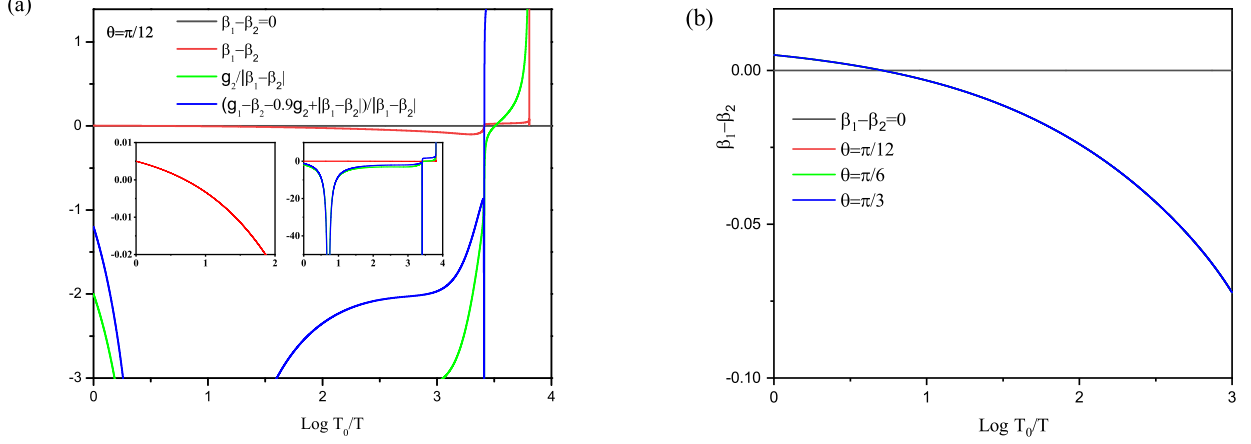


FIG. 8: (Color online) (a) Temperature-dependent stable constraints of the C_2 -symmetry DPMH state under the representative starting values of interaction parameters chosen as $g_1 = -0.015$, $g_2 = -0.01$, $u_s = 0.05$, $\lambda = 0.01$, $\beta_1 = 0.005$, $\beta_2 = 0.01$ (the qualitative results are insensitive to the initial values). Hereby, the angle θ is designated in Sec. II A to specify the direction of magnetic order in the spin space. Insets: the sign-change region of $\beta_1 - \beta_2$ (left panel) and enlarged-region for $\frac{g_1 - \beta_2}{|\beta_1 - \beta_2|} - \frac{9}{10} \frac{\bar{g}}{|\beta_1 - \beta_2|} + 1$ (right panel). (b) Sign-change regions of $\beta_1 - \beta_2$ under different values of θ .

$$\begin{aligned}
& +12\hat{g}[\mathcal{C}^3\mathcal{D}_1(a - \frac{\lambda a_s}{u_s})[\beta_2\mathcal{D}_1^2 + (\beta_1 - \beta_2)\mathcal{D}_2] + \mathcal{S}^3\mathcal{E}_1(a - \frac{\lambda a_s}{u_s})[\beta_2\mathcal{E}_1^2 + (\beta_1 - \beta_2)\mathcal{E}_2]] - \frac{\mathcal{D}_1\mathcal{E}_1(4a_s + 1)\lambda^2}{4} \\
& +8\mathcal{C}\mathcal{S}\hat{g}^2[2(\mathcal{C}\mathcal{D}_1(a - \frac{\lambda a_s}{u_s}) + \mathcal{S}\mathcal{E}_1(a - \frac{\lambda a_s}{u_s})) - 1] - \frac{\mathcal{F}^2(1 + 4a_s)\kappa^2}{4} - 3\hat{g}[\mathcal{C}^2[\beta_2\mathcal{D}_1^2 + (\beta_1 - \beta_2)\mathcal{D}_2] \\
& + \mathcal{S}^2[\beta_2\mathcal{E}_1^2 + (\beta_1 - \beta_2)\mathcal{E}_2]] + \frac{-2\mathcal{C}^2\mathcal{F}^2[\beta_2\mathcal{D}_1^2 + (\beta_1 - \beta_2)\mathcal{D}_2]a_s\kappa^2}{u_s}[1 - 2(2\mathcal{C}\mathcal{D}_1(a - \frac{\lambda a_s}{u_s}) - a_s)] \\
& + \frac{-2\mathcal{S}^2\mathcal{F}^2[\beta_2\mathcal{E}_1^2 + (\beta_1 - \beta_2)\mathcal{E}_2]a_s\kappa^2}{u_s}[1 - 2(2\mathcal{S}\mathcal{E}_1(a - \frac{\lambda a_s}{u_s}) - a_s)] - \frac{4\mathcal{C}^2\mathcal{S}^2\mathcal{F}^2\hat{g}^2a_s^2\kappa^2}{3u_s^2} \\
& \times [1 - 4(\mathcal{C}\mathcal{D}_1(a - \frac{\lambda a_s}{u_s}) + \mathcal{S}\mathcal{E}_1(a - \frac{\lambda a_s}{u_s}))] - \frac{3\mathcal{C}^2\mathcal{S}^2\mathcal{F}^2[\beta_2\mathcal{D}_1^2 + (\beta_1 - \beta_2)\mathcal{D}_2][\beta_2\mathcal{E}_1^2 + (\beta_1 - \beta_2)\mathcal{E}_2]a_s^2\kappa^2}{2u_s^2} \\
& \times [1 - 4(\mathcal{C}\mathcal{D}_1(a - \frac{\lambda a_s}{u_s}) + \mathcal{S}\mathcal{E}_1(a - \frac{\lambda a_s}{u_s}))] - \frac{\mathcal{C}^2\mathcal{S}^2\mathcal{F}^2\hat{g}^2a_s^2\kappa^2}{3u_s^2}[1 - 4(\mathcal{C}\mathcal{D}_1(a - \frac{\lambda a_s}{u_s}) + \mathcal{S}\mathcal{E}_1(a - \frac{\lambda a_s}{u_s}))]. \quad (\text{A13})
\end{aligned}$$

Furthermore, the RG equations of parameters β_1 and β_2 can be broken down into six distinct sorts depending on the concrete conditions.

For type-II case-A with $|\mathbf{n}_X^2|^2 = |\mathbf{n}_X|^4$, $|\mathbf{n}_Y^2|^2 = |\mathbf{n}_Y|^4$, $|\mathbf{n}_Y^2|^2 = 0$ and $|\mathbf{n}_X^2|^2 \neq 0$, β_1 evolves but β_2 is an invariant constant,

$$\begin{aligned}
\frac{d\beta_1}{dl} = & \beta_1 + \frac{2}{2\pi^2} \left\{ \frac{-4\mathcal{C}^2\mathcal{D}_1^2a_s\lambda^2\beta_1}{u_s}[1 - 2(2\mathcal{C}\mathcal{D}_1(a - \frac{\lambda a_s}{u_s}) - a_s)] + 9\mathcal{C}^2\mathcal{D}_2\beta_1^2[4\mathcal{C}\mathcal{D}_1(a - \frac{\lambda a_s}{u_s}) - 1] - \frac{\lambda^2(1 + 4a_s)}{4} \right. \\
& + \frac{\mathcal{S}^2\hat{g}^2}{\mathcal{D}_2}[4\mathcal{S}\mathcal{E}_1(a - \frac{\lambda a_s}{u_s}) - 1] - \frac{4\mathcal{C}\mathcal{D}_1a_s\lambda^3}{3u_s}[1 - 2(\mathcal{C}\mathcal{D}_1(a - \frac{\lambda a_s}{u_s}) - 2a_s)] \\
& \left. - \frac{2\mathcal{S}^2\mathcal{F}^2a_s\kappa^2\hat{g}}{3\mathcal{D}_2u_s}[1 - 2(2\mathcal{S}\mathcal{E}_1(a - \frac{\lambda a_s}{u_s}) - a_s)] \right\}, \quad (\text{A14})
\end{aligned}$$

$$\frac{d\beta_2}{dl} = 0. \quad (\text{A15})$$

For type-II case-B with $|\mathbf{n}_X^2|^2 = |\mathbf{n}_X|^4$, $|\mathbf{n}_Y^2|^2 = |\mathbf{n}_Y|^4$, $|\mathbf{n}_X^2|^2 = 0$ and $|\mathbf{n}_Y^2|^2 \neq 0$, β_1 evolves whereas β_2 is an invariant constant,

$$\begin{aligned}
\frac{d\beta_1}{dl} = & \beta_1 + \frac{2}{2\pi^2} \left\{ \frac{-4\mathcal{S}^2\mathcal{E}_1^2a_s\lambda^2\beta_1}{u_s}[1 - 2(2\mathcal{S}\mathcal{E}_1(a - \frac{\lambda a_s}{u_s}) - a_s)] - 9\mathcal{S}^2\mathcal{E}_2\beta_1^2[1 - 4\mathcal{S}\mathcal{E}_1(a - \frac{\lambda a_s}{u_s})] - \frac{\lambda^2(1 + 4a_s)}{4} \right. \\
& \left. + \frac{\mathcal{C}^2\hat{g}^2}{\mathcal{E}_2}[4\mathcal{C}\mathcal{D}_1(a - \frac{\lambda a_s}{u_s}) - 1] - \frac{4\mathcal{S}\mathcal{E}_1a_s\lambda^3}{3u_s}[1 - 2(\mathcal{S}\mathcal{E}_1(a - \frac{\lambda a_s}{u_s}) - 2a_s)] \right\}
\end{aligned}$$

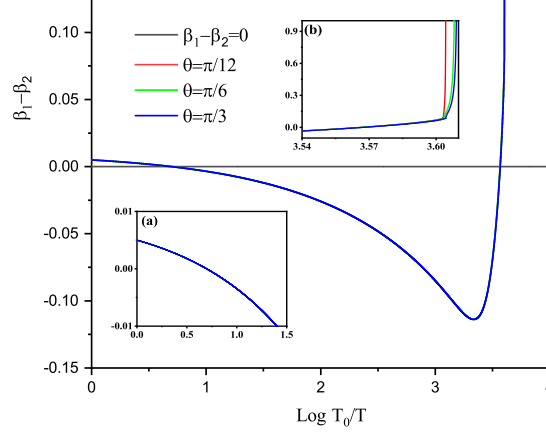


FIG. 9: (Color online) Temperature-dependent stable constraints ($\beta_1 - \beta_2$) of the C_2 -symmetry MH state under the representative starting values of interaction parameters chosen as $g_1 = 0.01$, $g_2 = -0.01$, $u_s = 0.05$, $\lambda = 0.01$, $\beta_1 = 0.01$, $\beta_2 = 0.005$ with three representative $\theta = \pi/12, \pi/6, \pi/3$ to satisfy the MH's stable constraint (the qualitative results are insensitive to the initial values). Hereby, the angle θ is designated in Sec. II A to specify the direction of magnetic order in the spin space. Insets: (a) the sign-change region of $\beta_1 - \beta_2$ and (b) behaviors around l_c .

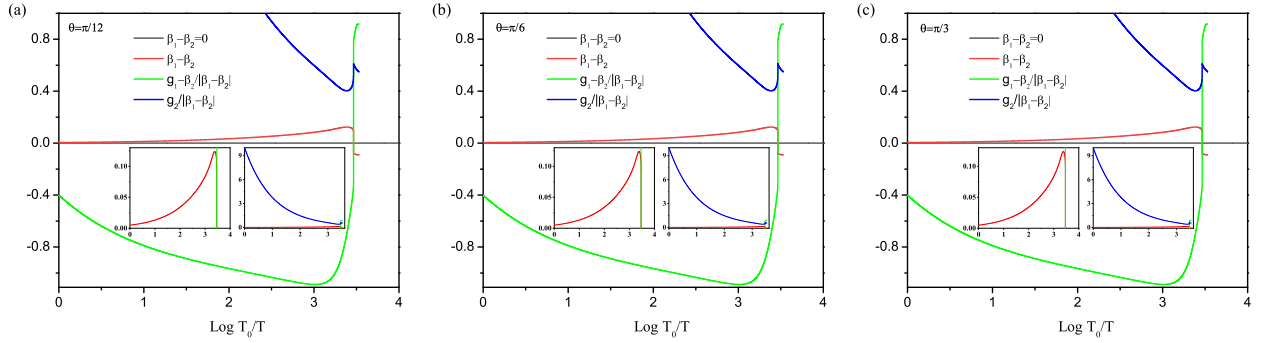


FIG. 10: (Color online) Temperature-dependent stable constraints of the C_2 -symmetry ICS \perp MH state under the representative starting values of interaction parameters chosen as $g_1 = 0.03$, $g_2 = 0.05$, $u_s = 0.05$, $\lambda = 0.01$, $\beta_1 = 0.01$, $\beta_2 = 0.005$ with three representative $\theta = \pi/12, \pi/6, \pi/3$ to satisfy the ICS \perp MH's stable constraint (the qualitative results are insensitive to the initial values). Hereby, the angle θ is designated in Sec. II A to specify the direction of magnetic order in the spin space: (a) $\theta = \pi/12$, (b) $\theta = \pi/6$, and (c) $\theta = \pi/3$. Insets: the enlarged regions for $\beta_1 - \beta_2$ (left panel) and $g_2/|\beta_1 - \beta_2|$ (right panel).

$$-\frac{2\mathcal{C}^2\mathcal{F}^2a_s\kappa^2\hat{g}}{3\mathcal{E}_2u_s}[1 - 2(2\mathcal{C}\mathcal{D}_1(a - \frac{\lambda a_s}{u_s}) - a_s)]\Big\}, \quad (\text{A16})$$

$$\frac{d\beta_2}{dl} = 0. \quad (\text{A17})$$

For type-II case-C with $|\mathbf{n}_X^2|^2 = |\mathbf{n}_X|^4$, $|\mathbf{n}_Y^2|^2 \neq |\mathbf{n}_Y|^4$, $|\mathbf{n}_Y^2|^2 = 0$, and $|\mathbf{n}_X^2|^2 = 0$, β_2 evolves but β_1 is an invariant constant,

$$\frac{d\beta_1}{dl} = 0, \quad (\text{A18})$$

$$\begin{aligned} \frac{d\beta_2}{dl} = & \beta_2 + \frac{2}{2\pi^2} \left\{ \frac{-4\mathcal{S}^2a_s\lambda^2[\beta_2\mathcal{E}_1^2 + (\beta_1 - \beta_2)\mathcal{E}_2]}{u_s} [1 - 2(2\mathcal{S}\mathcal{E}_1(a - \frac{\lambda a_s}{u_s}) - a_s)] - 9\mathcal{S}^2\beta_2^2\mathcal{E}_1^2[1 - 4\mathcal{S}\mathcal{E}_1(a - \frac{\lambda a_s}{u_s})] \right. \\ & + \frac{\mathcal{C}^2\hat{g}^2}{\mathcal{E}_1^2} [4\mathcal{C}\mathcal{D}_1(a - \frac{\lambda a_s}{u_s}) - 1] - \frac{4\mathcal{S}\mathcal{E}_1a_s\lambda^3}{3u_s} [1 - 2(\mathcal{S}\mathcal{E}_1(a - \frac{\lambda a_s}{u_s}) - 2a_s)] - \frac{\lambda^2(1 + 4a_s)}{4} \\ & \left. - \frac{2\mathcal{C}^2\mathcal{F}^2a_s\kappa^2\hat{g}}{3\mathcal{E}_1^2u_s} [1 - 2(2\mathcal{C}\mathcal{D}_1(a - \frac{\lambda a_s}{u_s}) - a_s)] \right\}. \end{aligned} \quad (\text{A19})$$

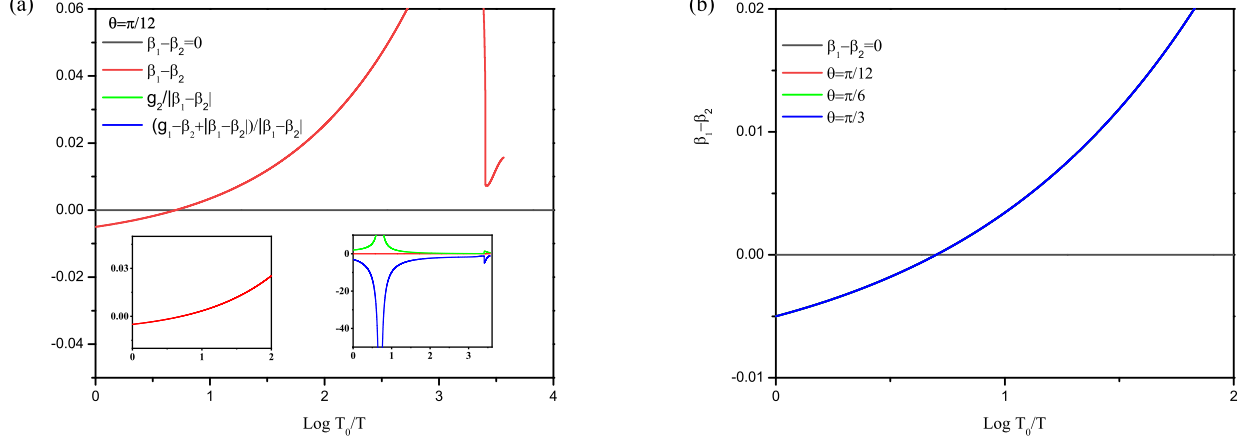


FIG. 11: (Color online) (a) Temperature-dependent stable constraints of C_4 -symmetry SVC state under the representative starting values of interaction parameters chosen as $g_1 = -0.01$, $g_2 = 0.01$, $u_s = 0.05$, $\lambda = 0.01$, $\beta_1 = 0.005$, $\beta_2 = 0.01$ with three representative $\theta = \pi/12, \pi/6, \pi/3$ to satisfy the SVC's stable constraint (the qualitative results are insensitive to initial values of parameters). Hereby, the angle θ is designated in Sec. II A to specify the direction of magnetic order in the spin space. Inset: the enlarge region for $g_2/|\beta_1 - \beta_2|$ and $(g_1 - \beta_2 + |\beta_1 - \beta_2|)/|\beta_1 - \beta_2|$. (b) Sign-change regions at different values of θ .

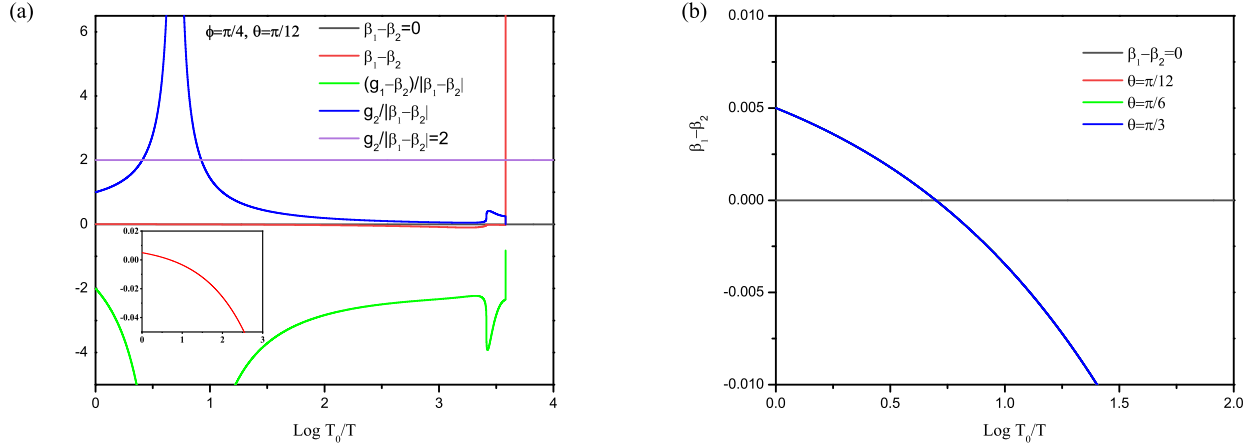


FIG. 12: (Color online) (a) Temperature-dependent stable constraints of symmetric double- \mathbf{Q} noncoplanar SWC state under the representative starting values of interaction parameters chosen as $g_1 = -0.005$, $g_2 = 0.005$, $u_s = 0.05$, $\lambda = 0.01$, $\beta_1 = 0.01$, $\beta_2 = 0.005$ with three representative $\theta = \pi/12, \pi/6, \pi/3$ to satisfy the symmetric SWC's stable constraint (the qualitative results are insensitive to initial values of parameters). Hereby, the angle θ is designated in Sec. II A to specify the direction of magnetic order in the spin space. In addition, ϕ is introduced by $\mathbf{n}_X \cdot \mathbf{n}_Y = \sin^2 \phi$ and $\phi = \pi/4$ corresponds to the symmetric noncoplanar SWC [19]. Inset: the enlarge region for $\beta_1 - \beta_2$. (b) Sign-change regions at different values of θ .

For type-II case-D with $|\mathbf{n}_Y^2|^2 = |\mathbf{n}_Y|^4$, $|\mathbf{n}_X^2|^2 \neq |\mathbf{n}_X|^4$, $|\mathbf{n}_Y^2|^2 = 0$, and $|\mathbf{n}_X^2|^2 = 0$, β_2 evolves but β_1 is an invariant constant,

$$\frac{d\beta_1}{dl} = 0, \quad (\text{A20})$$

$$\begin{aligned} \frac{d\beta_2}{dl} = & \beta_2 + \frac{2}{2\pi^2} \left\{ \frac{-4C^2 a_s \lambda^2 [\beta_2 \mathcal{D}_1^2 + (\beta_1 - \beta_2) \mathcal{D}_2]}{u_s} [1 - 2(2C\mathcal{D}_1(a - \frac{\lambda a_s}{u_s}) - a_s)] + 9C^2 \beta_2^2 \mathcal{D}_1^2 [4C\mathcal{D}_1(a - \frac{\lambda a_s}{u_s}) - 1] \right. \\ & + \frac{S^2 \hat{g}^2}{\mathcal{D}_1^2} [4S\mathcal{E}_1(a - \frac{\lambda a_s}{u_s}) - 1] - \frac{\lambda^2(1 + 4a_s)}{4} - \frac{4C\mathcal{D}_1 a_s \lambda^3}{3u_s} [1 - 2(C\mathcal{D}_1(a - \frac{\lambda a_s}{u_s}) - 2a_s)] \\ & \left. - \frac{2S^2 \mathcal{F}^2 a_s \kappa^2 \hat{g}}{3\mathcal{D}_1^2 u_s} [1 - 2(2S\mathcal{E}_1(a - \frac{\lambda a_s}{u_s}) - a_s)] \right\}. \end{aligned} \quad (\text{A21})$$

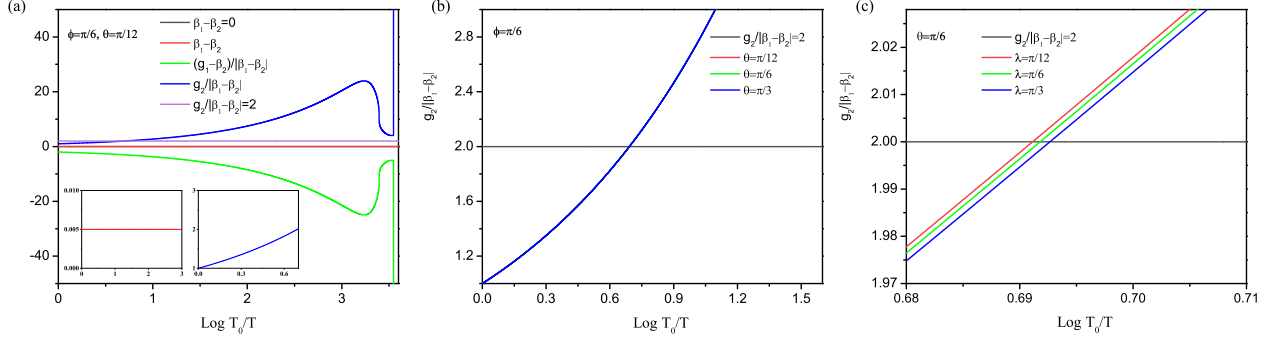


FIG. 13: (Color online) (a) Temperature-dependent stable constraints of asymmetric double- \mathbf{Q} noncoplanar SWC state under the representative starting values of interaction parameters chosen as $g_1 = -0.005$, $g_2 = 0.005$, $u_s = 0.05$, $\lambda = 0.01$, $\beta_1 = 0.01$, $\beta_2 = 0.005$ with three representative $\theta = \pi/12, \pi/6, \pi/3$ to satisfy the asymmetric SWC's stable constraint (the qualitative results are insensitive to initial values of parameters). Hereby, the angle θ is designated in Sec. II A to specify the direction of magnetic order in the spin space. In addition, ϕ is introduced by $\mathbf{n}_X \cdot \mathbf{n}_Y = \sin^2 \phi$ and a concrete value $\phi = \pi/6$ for the asymmetric case is taken [19]. Inset: the enlarge region for $\beta_1 - \beta_2$. (b) and (c) Sign-change regions at different values of θ and λ .

For type-II case-E with $|\mathbf{n}_Y|^2 \neq |\mathbf{n}_X|^4$, $|\mathbf{n}_X|^2 \neq |\mathbf{n}_X|^4$, $|\mathbf{n}_Y|^2 = 0$, and $|\mathbf{n}_X|^2 = 0$, β_2 evolves but β_1 is an invariant constant,

$$\frac{d\beta_1}{dl} = 0, \quad (\text{A22})$$

$$\begin{aligned} \frac{d\beta_2}{dl} = & \beta_2 + \frac{2}{2\pi^2} \left\{ \frac{-4C^2 a_s \lambda^2 [\beta_2 \mathcal{D}_1^2 + (\beta_1 - \beta_2) \mathcal{D}_2]}{u_s} [1 - 2(2C\mathcal{D}_1(a - \frac{\lambda a_s}{u_s}) - a_s)] + 9C^2 \beta_2^2 \mathcal{D}_1^2 [4C\mathcal{D}_1(a - \frac{\lambda a_s}{u_s}) - 1] \right. \\ & + \frac{\mathcal{S}^2 \hat{g}^2}{\mathcal{D}_1^2} [4\mathcal{S}\mathcal{E}_1(a - \frac{\lambda a_s}{u_s}) - 1] - \frac{\lambda^2(1 + 4a_s)}{4} - \frac{4C\mathcal{D}_1 a_s \lambda^3}{3u_s} [1 - 2(C\mathcal{D}_1(a - \frac{\lambda a_s}{u_s}) - 2a_s)] \\ & \left. - \frac{2\mathcal{S}^2 \mathcal{F}^2 a_s \kappa^2 \hat{g}}{3\mathcal{D}_1^2 u_s} [1 - 2(2\mathcal{S}\mathcal{E}_1(a - \frac{\lambda a_s}{u_s}) - a_s)] \right\}. \end{aligned} \quad (\text{A23})$$

For type-II case-F with $\mathcal{E}_2 \mathcal{D}_1^2 - \mathcal{D}_2 \mathcal{E}_1^2 = 0$, both β_1 and β_2 are energy-independent constants,

$$\frac{d\beta_1}{dl} = 0, \quad \frac{d\beta_2}{dl} = 0. \quad (\text{A24})$$

Appendix B: Stabilities of incommensurate magnetic states

As aforementioned in Sec. I of maintext, there are seven different types of IC magnetic states other than three commensurate ones including stripe SDW, CSDW, and SVC [16, 17, 33, 34]. To be concrete, these IC magnetic states cover four different C_2 IC cases consisting of C_2 IC ICS, C_2 MH, C_2 ICS \perp MH, and C_2 DPMH, as well as three distinct C_4 IC situations involving C_4 IC CSDW, C_4 IC SVC, and C_4 IC SWC [19]. In order to examine whether these IC magnetic states are stable against the decrease of energy scales, we within this section lean upon the coupled RG equations (A2)-(A24), which are completely encoded with the information of ordering competition, in conjunction with their stable constraints catalogued in Table I of the maintext.

In principle, the energy variable of RG evolution is expressed by $\Lambda = \Lambda_0 e^{-l}$ with $l > 0$ denoting the running scale. As our study is concerned with the structure of schematic phase diagram, it is herein of remarkable convenience to associate l with temperature via designating $T = T_0 e^{-l}$ with T_0 being the initial temperature to measure the evolution of energy scale [18, 31, 35–44]. On the basis of this transformation and RG equations in conjunction with the strategy addressed in Sec. III A, we are now in a proper position to judge whether these IC magnets are good candidates residing in the phase diagram of $\text{Ba}_{1-x}\text{Na}_x\text{Fe}_2\text{As}_2$ one by one.

We start out by considering the C_2 IC magnetic states. On one hand, the configurations of spin vectors for C_2 ICS magnetic state read $\mathbf{n}_X = (0, 0, 1)$ and $\mathbf{n}_Y = (0, 0, 0)$ [19], which satisfy the restricted conditions of type-II case-A. This indicates the interaction param-

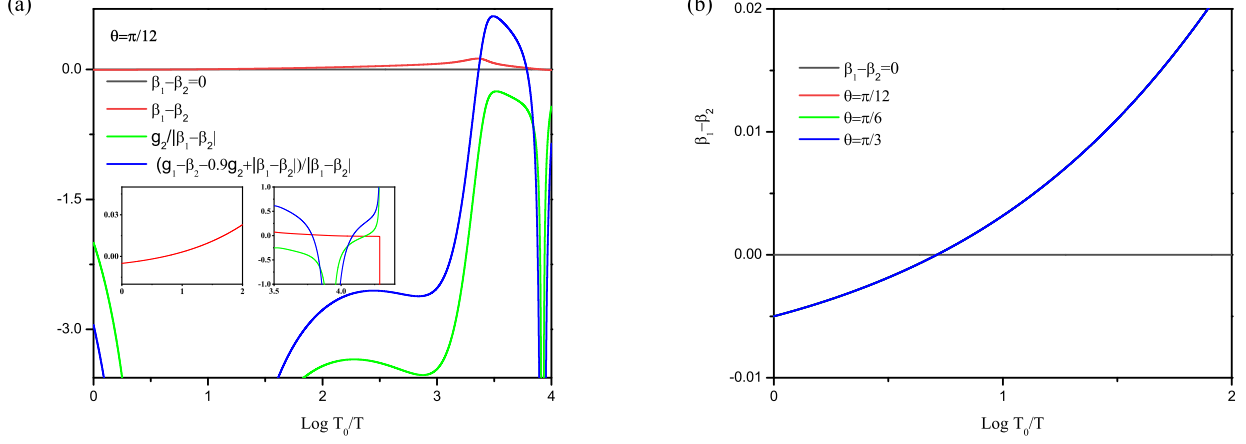


FIG. 14: (Color online) (a) Temperature-dependent stable constraints C_4 -symmetry IC CSDW state for case-1 under the representative starting values of interaction parameters chosen as $g_1 = -0.015$, $g_2 = -0.01$, $u_s = 0.05$, $\lambda = 0.01$, $\beta_1 = 0.005$, $\beta_2 = 0.01$ with three representative $\theta = \pi/12, \pi/6, \pi/3$ to satisfy the IC CSDW's stable constraint (the qualitative results are insensitive to initial values of parameters). Hereby, the angle θ is designated in Sec. II A to specify the direction of magnetic order in the spin space. Inset: the sign-change region of $(g_2 + |\beta_1 - \beta_2|)/|\beta_1 - \beta_2|$. (b) Sign-change regions at different values of θ .

ters obey the RG evolutions of type-II case-A delineated in Eqs. (A2)-(A5), (A8), (A9), and (A13)-(A15). As for C_2 ICS, its stable constraints can be either $(\beta_1 - \beta_2) < 0$, $g_2/|\beta_1 - \beta_2| > 0$, $(g_1 - \beta_2)/|\beta_1 - \beta_2| > -1$ or $(\beta_1 - \beta_2) < 0$, $g_2/|\beta_1 - \beta_2| < 0$, $(g_1 - \beta_2 - 0.9g_2)/|\beta_1 - \beta_2| > -1$ [19]. Based on these, we perform numerical RG analysis by taking some initial representative values of parameters and obtain the results shown in Fig. 4. On the other, concerning C_2 MH and C_2 DPMH, the configurations of spin vectors are characterized by $\mathbf{n}_X = \frac{1}{\sqrt{2}}(i, 0, 1)/$, $\mathbf{n}_Y = (0, 0, 0)$, and $\mathbf{n}_X = \frac{1}{\sqrt{2}}(i, 0, 1)$, $\mathbf{n}_Y = \frac{1}{\sqrt{2}}(i, 0, 1)$, respectively [19]. Accordingly, this indicates that the interaction parameters are dictated by the evolutions for type-II case-D provided in Eqs. (A2)-(A5), (A8), (A9), (A13), and (A20)-(A21). To proceed, we parallel the analogous RG numerical analysis taking advantage of the corresponding constraints [19] $(\beta_1 - \beta_2) > 0$, $g_2/|\beta_1 - \beta_2| > 0$, $(g_1 - \beta_2)/|\beta_1 - \beta_2| > 0$ or $(\beta_1 - \beta_2) > 0$, $g_2/|\beta_1 - \beta_2| < 0$, $(g_1 - \beta_2 - 0.9g_2)/|\beta_1 - \beta_2| > -1$ for C_2 MH and $(\beta_1 - \beta_2) > 0$, $g_2/|\beta_1 - \beta_2| < 0$, $(g_1 - \beta_2 - 0.9g_2)/|\beta_1 - \beta_2| < -1$ for C_2 DPMH, respectively. The conclusions are underscored in Fig. 8 and Fig. 9 with taking some representative beginning values of parameters. Learning from Fig. 4, Fig. 8, and Fig. 9, we apparently figure out that the sign change of $\beta_1 - \beta_2$ is occurred explicitly once temperature is slightly lowered owing to the effects of ordering competition. As a consequence, we infer that C_2 ICS, C_2 MH and C_2 DPMH are not stable states in the low-energy regime and hence not good candidates for IC magnetic state nearby the QCP in phase diagram of $\text{Ba}_{1-x}\text{Na}_x\text{Fe}_2\text{As}_2$. However, these three C_2 IC states might be suitable states for the quantum critical region with high temperatures, such as C_2 IC SDW illustrated

in Fig. 1.

In a sharp contrast, with respect to C_2 ICS \perp MH, whose the configurations of spin vectors are related to $\mathbf{n}_X = (0, 0, 1)$ and $\mathbf{n}_Y = \frac{1}{\sqrt{2}}(i, 1, 0)$ [19], their interaction parameters are therefore subject to type-I coupled RG equations (A2)-(A10). Carrying out the similar numerical analysis gives rise to temperature-dependent evolutions depicted in Fig. 10. It manifestly heralds that stable constraints of C_2 ICS \perp MH, i.e., $(\beta_1 - \beta_2) > 0$, $(g_1 - \beta_2)/|\beta_1 - \beta_2| < 0$, and $g_2/|\beta_1 - \beta_2| > f(g_1 - \beta_2) \approx 2$ for a finite value of $g_1 - \beta_2$ and $\lim_{(g_1 - \beta_2) \rightarrow 0} f(g_1 - \beta_2) \rightarrow 0$ [19], are remarkably robust against ordering competition as the temperature is decreased. Despite of relative stability, it is very necessary to point out that C_2 ICS \perp MH can be destroyed as long as the magnetic QCP is closely accessed, at which the ordering competition becomes so ferocious that any state cannot present solely.

Next, we go to judge C_4 IC magnetic states, which include C_4 IC SVC, C_4 SWC, and C_4 IC CSDW. In analogy to C_2 IC magnetic states, we inspect low-energy fates of these states by combining their RG equations and stable constraints. For C_4 IC SVC with the configurations of spin vectors being $\mathbf{n}_X = (0, 0, 1)$ and $\mathbf{n}_Y = (0, 1, 0)$ [19], the interaction parameters are governed by the type-II case-A RG equations (A2)-(A5), (A8), (A9), (A13)-(A15) and the stable constraints correspond to $(\beta_1 - \beta_2) < 0$, $g_2/|\beta_1 - \beta_2| > 0$, and $(g_1 - \beta_2)/|\beta_1 - \beta_2| < -1$ [19]. The numerical results presented in Fig. 11 reflect that C_4 IC SVC cannot be a well stable state in the phase diagram caused by the influence of ordering competition.

To proceed, we turn to C_4 IC SWC, which is well protected by constraints $(\beta_1 - \beta_2) > 0$, $(g_1 - \beta_2)/|\beta_1 - \beta_2| < 0$, and $0 < g_2/|\beta_1 - \beta_2| < 2$ [19]. In addition, the

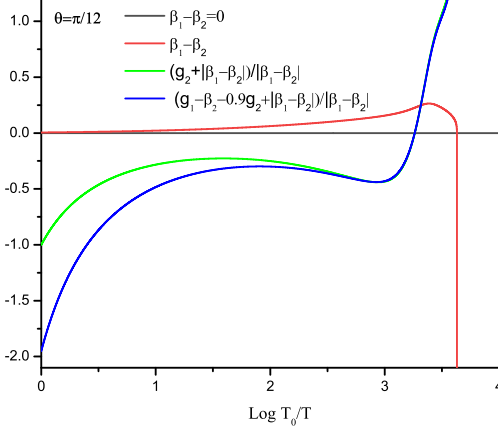


FIG. 15: (Color online) Temperature-dependent stable constraints C_4 -symmetry IC CSDW state for case-2 under the representative starting values of interaction parameters chosen as $g_1 = -0.015$, $g_2 = -0.01$, $u_s = 0.05$, $\lambda = 0.01$, $\beta_1 = 0.01$, $\beta_2 = 0.005$ with a representative $\theta = \pi/12$ to satisfy the IC CSDW's stable constraint (the qualitative results are insensitive to initial values of parameters). Hereby, the angle θ is designated in Sec. II A to specify the direction of magnetic order in the spin space.

configurations of spin vectors are equivalent to $\mathbf{n}_X = (i \cos \phi, 0, \sin \phi)$ and $\mathbf{n}_Y = (0, i \cos \phi, \sin \phi)$. Before going further, it is of particular interest to address that they can be clustered into two sub-situations distinguished by the parameter ϕ which is introduced by $\mathbf{n}_X \cdot \mathbf{n}_Y = \sin^2 \phi$ and characterize the symmetric double- \mathbf{Q} noncoplanar

SWC with $\phi = \pi/4$ and asymmetric double- \mathbf{Q} noncoplanar with $\phi \neq \pi/4$, respectively [19]. As a result, the former interaction parameters are dictated by type-II case-A RG equations (A2)-(A5), (A8), (A9), and (A13)-(A15) but instead the latter ones evolve under type-II case-F RG equations exhibited in Eqs. (A2)-(A5), (A8), (A9), (A13), and (A24). Carrying out analogous RG steps yields to Fig. 12 and Fig. 13, which explicitly signals C_4 SWC is not suitable to be present in the phase diagram.

Further, we move to C_4 IC CSDW state, at which the configurations of spin vectors are of the form $\mathbf{n}_X = (0, 0, 1)$ and $\mathbf{n}_Y = (0, 0, 1)$ [19], and thus type-II case-A RG equations (A2)-(A5), (A8), (A9), and (A13)-(A15) are in charge of the low-energy fates of interaction parameters. Hereby, it is necessary to highlight that C_4 -symmetry IC CSDW [19] can be stabilized by either $(\beta_1 - \beta_2) < 0$, $g_2/|\beta_1 - \beta_2| < 0$, $(g_1 - \beta_2 - 0.9g_2)/|\beta_1 - \beta_2| < -1$ (case-1) or $(\beta_1 - \beta_2) > 0$, $g_2/|\beta_1 - \beta_2| < -1$, $(g_1 - \beta_2 - 0.9g_2)/|\beta_1 - \beta_2| < -1$ (case-2). Fig. 14 and Fig. 15 collect the central results stemming from RG analysis, which manifestly exhibit the temperature (energy) dependence of associated parameters for C_4 IC CSDW. In the light of these figures, we are informed that stable constraints for both case-1 and case-2 are considerably robust with the decrease of temperature, which of course can be sabotaged due to sufficiently strong fluctuations so long as the magnetic QCP is closely approached. Consequently, C_4 IC CSDW, like its C_2 ICS \perp MH counterpart, is of fair robustness against ordering competition and an appropriate candidate for C_4 magnetic state in phase diagram of $\text{Ba}_{1-x}\text{Na}_x\text{Fe}_2\text{As}_2$.

-
- [1] D. S. Inosov *et al.*, Nat. Phys. **6**, 178 (2010); J. Paglione and R. L. Greene, Nat. Phys. **6**, 645 (2010); P. Dai, J. Hu, and E. Dagotto, Nat. Phys. **8**, 709 (2012).
 - [2] G. R. Stewart, Rev. Mod. Phys. **83**, 1589 (2011); E. Dagotto, Rev. Mod. Phys. **85**, 849 (2013); P. C. Dai, Rev. Mod. Phys. **87**, 855 (2015).
 - [3] I. R. Fisher, L. Degiorgi, and Z. X. Shen, Rep. Prog. Phys. **74**, 124506 (2011); H.-H. Kuo *et al.*, Science **352**, 958 (2016); P. J. Hirschfeld, M. M. Korshunov, and I. I. Mazin, Rep. Prog. Phys. **74**, 124508 (2011).
 - [4] M. G. Kim *et al.*, Phys. Rev. B **82**, 220503(R) (2010); S. Nandi *et al.*, Phys. Rev. Lett. **104**, 057006 (2010); E. Hassinger *et al.*, Phys. Rev. B **86**, 140502 (2012).
 - [5] S. Avci *et al.*, Nat. Commun. **5**, 3845 (2014).
 - [6] A. E. Böhrer, F. Hardy, L. Wang, T. Wolf, P. Schweiss, and C. Meingast, Nat. Commun. **6**, 7911 (2015).
 - [7] J. M. Allred *et al.*, Phys. Rev. B **92**, 094515 (2015); E. Hassinger *et al.*, Phys. Rev. B **93**, 144401 (2016); J. M. Allred *et al.*, Nat. Phys. **12**, 493 (2016).
 - [8] L. Wang, F. Hardy, A. E. Böhrer, T. Wolf, P. Schweiss, and C. Meingast, Phys. Rev. B **93**, 014514 (2016).
 - [9] M. N. Gastiasoro, I. Eremin, R. M. Fernandes and B. M. Andersen, Nat. Commun. **8**, 14317 (2017).
 - [10] M. Yi *et al.*, Phys. Rev. Lett. **121**, 127001 (2018); L. Wang *et al.*, Phys. Rev. B **97**, 224518 (2018).
 - [11] E. I. Timmons *et al.*, Phys. Rev. B **99**, 054518 (2019); R. Prozorov *et al.*, NPJ Quantum Materials **4**, 34 (2019).
 - [12] D. N. Basov and A. V. Chubukov, Nat. Phys. **7**, 272 (2011); R. M. Fernandes, A. V. Chubukov, and J. Schmalian, Nat. Phys. **10**, 97 (2014).
 - [13] A. V. Chubukov, Annu. Rev. Condens. Matter Phys. **3**, 57 (2012); R. M. Fernandes and A. V. Chubukov, Rep. Prog. Phys. **80**, 014503 (2017); R. M. Fernandes, P. P. Orth, and J. Schmalian, Annu. Rev. Condens. Matter Phys. **10**, 133 (2019).
 - [14] M. Vojta, Rep. Prog. Phys. **66**, 2069 (2003); S. Sachdev, Quantum Phase Transitions 1st ed. (Cambridge University Press, Cambridge, UK, 1999).
 - [15] X. Chen, S. Maiti, R. M. Fernandes, and P. J. Hirschfeld, Phys. Rev. B **102**, 184512 (2020).
 - [16] R. M. Fernandes, S. A. Kivelson, and E. Berg, Phys. Rev. B **93**, 014511 (2016).
 - [17] M. Hoyer, R. M. Fernandes, A. Levchenko, and J. Schmalian, Phys. Rev. B **93**, 144414 (2016).
 - [18] J. Wang, G.-Z. Liu, D. V. Efremov, and J. van den Brink,

- Phys. Rev. B **95**, 024511, (2017).
- [19] M. H. Christensen, B. M. Andersen, and P. Kotetes, Phys. Rev. X **8**, 041022 (2018).
 - [20] K. G. Wilson, Rev. Mod. Phys. **47** 773 (1975); J. Polchinski, arXiv: hep-th/9210046 (1992); R. Shankar, Rev. Mod. Phys. **66**, 129 (1994).
 - [21] I. Eremin and A. V. Chubukov, Phys. Rev. B **81**, 024511 (2010); J. Knolle, I. Eremin, A. V. Chubukov, and R. Moessner, Phys. Rev. B **81**, 140506(R) (2010).
 - [22] R. M. Fernandes, S. Maiti, P. Wölfle, and A. V. Chubukov, Phys. Rev. Lett. **111**, 057001 (2013); A. Levchenko, M. G. Vavilov, M. Khodas, and A. V. Chubukov, Phys. Rev. Lett. **110**, 177003 (2013).
 - [23] D. Chowdhury, B. Swingle, E. Berg, S. Sachdev, Phys. Rev. Lett. **111**, 157004 (2013).
 - [24] A. V. Chubukov, D. V. Efremov, and I. Eremin, Phys. Rev. B **78**, 134512 (2008); S. Maiti and A. V. Chubukov, Phys. Rev. B **82**, 214515 (2010).
 - [25] C. Fang, H. Yao, W.-F. Tsai, J. P. Hu, and S. A. Kivelson, Phys. Rev. B **77**, 224509 (2008); C. Xu, M. Muller, and S. Sachdev, Phys. Rev. B **78**, 020501(R) (2008).
 - [26] R. M. Fernandes *et al.*, Phys. Rev. Lett. **105**, 157003 (2010).
 - [27] H. J. Schulz, Phys. Rev. Lett. **64**, 1445 (1990).
 - [28] M. H. Christensen, D. D. Scherer, P. Kotetes, and B. M. Andersen, Phys. Rev. B **96**, 014523 (2017).
 - [29] B. I. Halperin, T. C. Lubensky, and S.-K. Ma, Phys. Rev. Lett. **32**, 292 (1974).
 - [30] H. Kleinert and F. S. Nogueira, Nucl. Phys. B **651**, 361 (2003).
 - [31] J. Wang and G.-Z. Liu, Phys. Rev. D **90**, 125015 (2014); J. Wang and G.-Z. Liu, Phys. Rev. B **92**, 184510 (2015).
 - [32] Besides a , a_s , u_s , λ , β_1 , β_2 , g_1 , and g_2 appearing in the free energy (1), κ and $\lambda_{\Delta A}$ are two additional fundamental parameters.
 - [33] R. Yu, M. Yi, B. A. Frandsen, R. J. Birgeneau, and Q. Si, arXiv:1706.07087v1 (2017).
 - [34] M. Klug, J. Kang, R. M. Fernandes, J. Schmalian, Phys. Rev. B **97**, 155130 (2018).
 - [35] R. M. Fernandes, A. V. Chubukov, J. Knolle, I. Eremin, and J. Schmalian, Phys. Rev. B **85**, 024534 (2012);
 - [36] L. Nandkishore, L. Levitov, and A. V. Chubukov, Nat. Phys. **8**, 158 (2012).
 - [37] J. -H. She, M. J. Lawler, and E. -A. Kim, Phys. Rev. B **92**, 035112 (2015).
 - [38] L. Savary, E. -G. Moon, and L. Balents, Phys. Rev. X **4**, 041027 (2014).
 - [39] A. Schliefl, P. Lunts, and S. -S. Lee, Phys. Rev. X **7**, 021010 (2017).
 - [40] Y. Huh and S. Sachdev, Phys. Rev. B **78**, 064512 (2008).
 - [41] C. Xu, Y. Qi, and S. Sachdev, Phys. Rev. B **78**, 134507 (2008).
 - [42] M. S. Foster and I. L. Aleiner, Phys. Rev. B **77**, 195413 (2008).
 - [43] A. V. Chubukov, M. Khodas, and R. M. Fernandes, Phys. Rev. X **6**, 041045 (2016).
 - [44] M. A. Metlitski, D. F. Mross, S. Sachdev, and T. Senthil, Phys. Rev. B **91**, 115111 (2015).
 - [45] M. W. Puga, E. Simanek, and H. Beck, Phys. Rev. B **26**, 2673 (1982).
 - [46] G.-Z. Liu, J.-R. Wang, and J. Wang, Phys. Rev. B **85**, 174525 (2012).
 - [47] A. E. Koshelev, Phys. Rev. B **102**, 054505 (2020).
 - [48] E. Helfand and N. R. Werthamer, Phys. Rev. **147**, 288 (1966).